Microelectronics Reliability 139 (2022) 114801

Contents lists available at ScienceDirect

Microelectronics Reliability

journal homepage: www.elsevier.com/locate/microrel

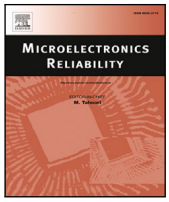

Ab initio investigations in amorphous silicon dioxide: Proposing a multi-state defect model for electron and hole capture

Christoph Wilhelmer [a,*], Dominic Waldhoer [b], Markus Jech [b], Al-Moatasem Bellah El-Sayed [b], Lukas Cvitkovich [b], Michael Waltl [a], Tibor Grasser [b]

[a] Christian Doppler Laboratory for Single-Defect Spectroscopy in Semiconductor Devices at the Institute for Microelectronics, TU Wien, Vienna, Austria
[b] Institute for Microelectronics, TU Wien, Gusshausstraße 27-29 Vienna, 1040, Austria

ARTICLE INFO

Keywords:
Ab initio studies in amorphous SiO_2
Nonradiative multi-phonon defect model
Oxygen vacancy
Hydrogen bridge
Hydroxyl-E' center
Electron/hole traps
Metastability of defects
Statistics of defect properties
MOSFET
Si/SiC substrates
Bias temperature instability
Random telegraph noise

ABSTRACT

Experiments as well as theoretical calculations indicate that point defects in the amorphous SiO_2 layer of electronic devices as well as in optical fibers are responsible for numerous stability and reliability phenomena, including noise, hysteresis, bias temperature instabilities and decreasing transmission efficiency. In addition to the well-known oxygen vacancy, hydrogen related defects such as the hydrogen bridge and the hydroxyl-E' center have gained a considerable amount of attention in the recent past, as they are suspected to negatively influence the device performance by capturing charge carriers from e.g. both Si and SiC substrates in field effect transistors. Here, we present a thorough *ab initio* study of these oxide defects and develop a unified description of electron and hole capture processes in a single multi-state model, supported by a comprehensive analysis of various defect parameters like relaxation energies, charge transition levels, (meta-)stability and transition barriers. We show that a single oxide defect can have two different trap levels for both electron and hole capturing processes, which might be the cause of anomalous device degradation phenomena. Based on its low formation energy compared to other defect types, we find that the hydroxyl-E' center is the most promising defect candidate to explain charge capture processes in Si/SiO_2 systems. Furthermore, we argue that the reduced effect of positive bias temperature instability (PBTI) observed in MOS devices compared to its negative counterpart (NBTI) can be explained by the locations of the hydroxyl-E' centers charge transition levels.

1. Introduction

Over the last decades, amorphous silicon dioxide (a-SiO_2) has played a major role in the fields of optics and electronics, being heavily used in industry as an optical fiber or as the gate oxide of metal–oxide–semiconductor field effect transistors (MOSFETs) respectively. As these devices can be produced in ever smaller dimensions, driven by the ongoing progresses in processing technologies, reliability issues are determined by atomic point defects, which are able to trap charges from the substrate or gate during operation. Even though defects in a-SiO_2 have been the focus of many theoretical and experimental studies in the past [1–7], many open questions concerning the intricate defect dynamics still remain, as investigations in this amorphous material are highly challenging because each single point defect is expected to behave differently, yielding individual defect "footprints". In particular, it is understood that the same defects can be involved in both hole and electron trapping process as visualized in the state diagram of a single hydrogen bridge (HB) defect in three charge states, including metastable configurations, in Fig. 1. Furthermore, due to transitions between stable and metastable defect configurations in the same charge state, defects may stay electrically inactive for a long time (even months) [8], which highlights the complexity of the involved defect dynamics and requires sophisticated models to be fully understood.

Although SiO_2 in scaled electronics has been steadily replaced by HfO_2 as the gate oxide due to its higher permittivity, even in ultra-scaled devices there is still a thin layer of SiO_2 present due to the oxidation of the Si surface by excess oxygen atoms during film growth and due to Si diffusion into the film [9,10]. Defects in this interfacial layer have a particularly strong impact on the device degradation because of their close proximity to the device channel and therefore often dominate the degradation [11] which motivates further investigations in SiO_2. While the hole trapping mechanism has already been examined at some depth using a four-state defect model [4,12–14] where the charge transfer reactions are characterized by a nonradiative multi-phonon (NMP) process while the thermal reconfigurations were described using transition state theory, a consistent description

* Corresponding author.
E-mail addresses: wilhelmer@iue.tuwien.ac.at (C. Wilhelmer), grasser@iue.tuwien.ac.at (T. Grasser).

https://doi.org/10.1016/j.microrel.2022.114801
Received 24 June 2022; Received in revised form 12 September 2022; Accepted 24 September 2022
Available online 17 October 2022

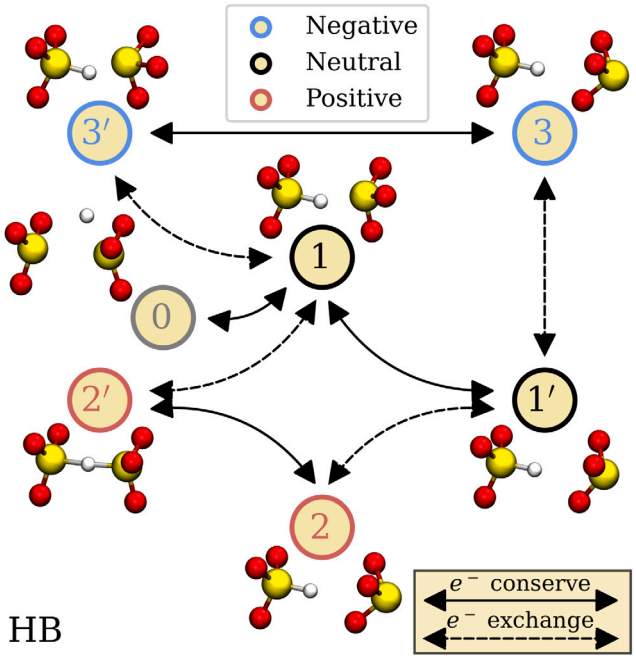

Fig. 1. Schematic state diagram of a hydrogen bride (HB) defect in the three charge states neutral (1 black), positive (2 red) and negative (3 blue). 0 (gray) denotes a precursor configuration with a preexisting oxygen vacancy and a H at an interstitial position before a HB defect is formed. Possible transitions between defect configurations in the same charge state are shown as full lines, transitions involving charge carrier exchange as dashed lines. Direct transitions between positively and negatively charged defects are theoretically possible but rather unlikely to occur as will be demonstrated in Section 3.5. Note that there also might be transitions outside of this state diagram, e.g. the hydrogen can also get detached from the defect, move to an interstitial position and subsequently form a new HB at a different position in the oxide.

including the electron trapping process is still missing. In addition to the various configurations of the well-known oxygen vacancy (OV) [3,15,16], which is unlikely to change its charge state in scaled Si devices due to its low charge trapping level ($\langle E_T \rangle - E_V(\mathrm{Si}) \sim 3\,\mathrm{eV}$) [17–19] but is suspected to be responsible for hole trapping in SiC devices [20], hydrogen related defects in SiO_2 have gained a lot of interest in the recent past in both electronics [12,21–23] as well as in optical fibers, where H is known to introduce losses by forming hydroxyl groups in the silica [24,25]. This is primarily because hydrogen is not only present during many fabrication processes but is also deliberately introduced in semiconductor devices during a forming gas anneal in order to passivate Si dangling bonds at the interface, which would otherwise drastically reduce the channel mobility and the ON/OFF ration of the device [26–29]. However, once introduced, hydrogen easily diffuses through the oxide [30–32] and can trigger detrimental reactions within the amorphous SiO_2 network, creating new defect types suspected to have charge transition levels (CTLs) near the band edges of Si and SiC substrates [12,20,33]. For example, H can create point defects in SiO_2 like the hydroxyl-E' center (H-E') [21,34,35], where a hydrogen attaches to and eventually breaks an already strained Si–O bond, thereby forming a hydroxyl group. Hydrogen can also interact with preexisting defects, e.g. by forming an active hydrogen bridge from an oxygen vacancy [15,36–39].

The schematic potential energy curves (PECs) of an oxide defect in three different charge states including metastable configurations are shown in the context of a Si/SiO_2 band diagram in Fig. 2 containing the trap levels E_T and the relaxation energies E_{Relax}. The corresponding states from Fig. 1 are aligned with the local minima of the PEC. Hereby, the valence band maximum (VBM) and conduction band minimum (CBM) of the Si substrate act as charge reservoirs. Nonradiative charge capture events are expected to occur over the crossing point of two energy curves in the classical high temperature limit. The hole trapping mechanism is shown in Fig. 2 (left) where the defect is initially neutral with equilibrium energy E^0. By trapping a hole from the VBM, the defect becomes positively charged, which corresponds to a local energy minimum of the positive PEC E^+, and subsequently relaxes to a new stable configuration by overcoming a small thermal barrier, depicted as the transition state (TST). This process corresponds to the transitions $1 \rightarrow 2' \rightarrow 2$ as also illustrated in Fig. 1. The same concept can be applied to the electron trapping mechanism as shown in Fig. 2 (right).

In addition to the PECs in the various charge states, which determine the transition probabilities, we will also calculate the formation energy E_{Form} of each defect with respect to their precursor atomic configurations to estimate the concentration of each type. Based on these results, we show that of all defect candidates considered here the H-E' center is expected to have the largest concentration in SiO_2. We improve the accuracy of previously published defect parameters concerning hole trapping [19,35] by performing density functional theory (DFT) cell relaxations to release the internal stress of our a-SiO_2 structures before calculating the defect properties. To analyze the PEC of the defects, we examine the relaxation energy E_{Relax} for the charge transitions 0/+, 0/−, +/0 and −/0 as well as −/+ and +/− and calculate the CTLs with respect to the VBM of SiO_2 for each kind of defect. We show by transition barrier calculations that a Si, fivefold coordinated with four O and one H, is a ground state of the H-E' in the negative charge state. This ground state exhibits charge transition levels for electron trapping far below the CBM of a Si bulk, which can explain the reduced electron trapping in Si based MOS devices leading to phenomena like bias temperature instability (BTI) compared to the much more pronounced hole trapping. We calculate energy barriers for different charge transition processes employing the harmonic PEC approximation, showing that a charge transition −/0 (+/0) is energetically always favored compared to a −/+ (+/−) transition. Metastable defect configurations are discovered and analyzed by statistical evaluation of the total energy differences between stable and metastable configurations and the energy barriers for a transition between them. Distinct CTLs of multi-state defects are correlated against each other to give an explanation for different charge trapping timescales of single defects. Furthermore, correlations of a defect's CTL with its structural properties and formation energy are investigated to analyze the impact of the theoretically calculated trapping ability on the actual device performance. This theoretical study offers a statistical insight into defects in SiO_2 aiming to describe hole and electron capture processes in a unified multi-state defect model.

2. Methodology

In the following we present our computational setup as well as the methods used to obtain the results in this work in detail.

2.1. DFT setup

All DFT calculations were carried out in a single structure of a-SiO_2 containing 216 atoms with three-dimensional periodic boundary conditions applied to the system. The calculations were performed using the Gaussian plane wave (GPW) method as implemented in the CP2K code [40]. We use the Goedecker–Teter–Hutter (GTH) pseudopotentials [41] in combination with a double-ζ Gaussian basis set [42] and employ an energy cutoff of 800 Ry for the plane wave expansion of the electron density. To accurately calculate the electronic structure and to minimize the errors of electronic state calculations in the bandgap of the defect system, the non-local hybrid functional PBE0_TC_LRC [43] was used for all calculations. We additionally use the auxiliary basis set pFIT3 to mitigate computational costs of calculating the Hartree–Fock exchange [44]. The total energy of the system was converged self-consistently up to 2.7×10^{-6} eV. Energy barriers were calculated with the climbing image nudged elastic band method (CI-NEB) [45] employing the PBE functional and using 7 intermediate images each.

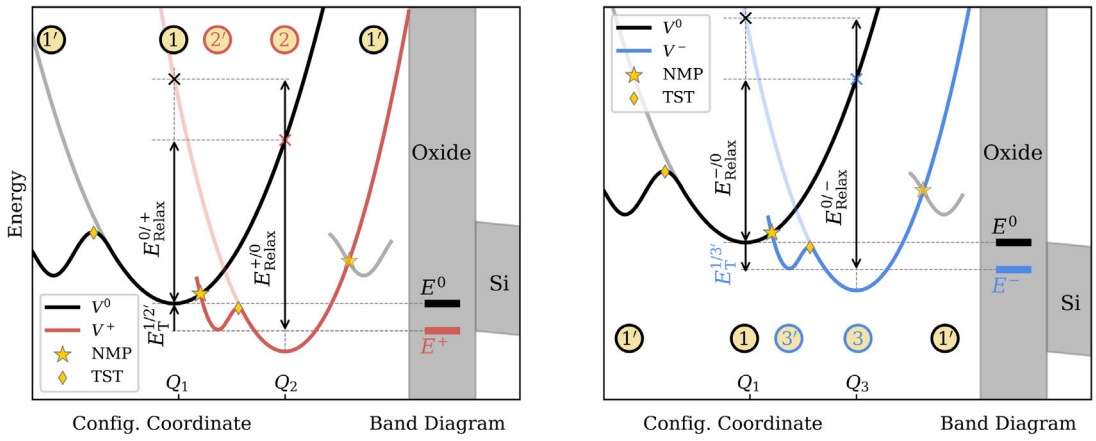

Fig. 2. Schematic potential energy curves of a four-state oxide defect as a function of the configuration coordinate Q_i for the +/0 (left) and −/0 (right) charge transitions in the context of a Si/SiO_2 band diagram. The stable and metastable configurations states are denoted according to the state diagram in Fig. 1. The harmonic approximation is shown as a transparent line for the stable configurations with the relaxation energies E_{Relax} and the trap levels E_{T} for all investigated charge transitions depicted as the according energy differences. The crossing point of two energy curves in different charge states according to the nonradiative multi phonon model is shown as a star while classical transition states (TST) for charge conserving transitions are depicted with a diamond. By applying a bias, the energy levels can be shifted against each other.

2.2. SiO_2 structure creation

20 amorphous SiO_2 structures containing 216 atoms were created by simulated melting and subsequent quenching of β-cristobalite as already successfully carried out in previous publications [12]. This specific SiO_2 polymorph was used as its density (2.33 g cm^{-3}) is closer to a-SiO_2 (2.2 g cm^{-3}) compared to α-quartz (2.65 g cm^{-3}). Molecular dynamics (MD) as implemented in the LAMMPS code [46] was deployed using the classical ReaxFF potential [47], calibrated towards Si/SiO_2 systems. This force field was proven in previous publications to be an excellent choice due to its ability to dynamically break and form bonds [22]. We employed the Verlet algorithm to propagate the system in time using a time step of 0.1 fs. The system was heated up above its melting point to 5000 K and kept at this temperature for full randomization and afterwards cooled down to 0 K at a rate of 6 K ps^{-1}. The obtained structures were further relaxed within DFT to reduce internal forces to 0.025 eV/Å. Additionally, the cell parameters were also allowed to change during relaxation to remove any residual mechanical stress in the structures (down to 0.01 GPa). This cell relaxation improves the soundness of the defect calculations compared to our previous works where structures were stills slightly strained. Geometry optimizations in different charge states q were performed on the structures using the Broyden–Fletcher–Goldfarb–Shanno (BFGS) algorithm [48–51].

2.3. Structural analysis

The distributions of the Si–O bond lengths and the O–Si–O and Si–O–Si angles across all 20 structures created with our setup are shown in Fig. 3. Bond lengths (1.63 ± 0.02 Å) and angles (O–Si–O = 109.47 ± 4.26 ° and Si–O–Si = 143.41 ± 13.2 °) are in the same range as previous DFT calculations [5] and are in good agreement with high-energy X-ray and neutron diffraction measurements [2,52]. The average mass density of the structures is 2.17 g cm^{-3}, which also agrees well with experimental data for SiO_2 thin films on Si [53]. The following defect calculations were carried out on a single structure characterized by structural parameters consistent with the distribution over all 20 structures. For this structure, all Si atoms are fourfold coordinated with O and all O atoms are twofold coordinated with Si. Its structural parameters are shown as blue bins in Fig. 3. In a-SiO_2, characteristic geometrical distances like bond lengths cannot be measured directly by X-ray diffraction, as Bragg's law cannot be applied in amorphous materials. Nonetheless, the structure factor S [54], which gives information about the short-, medium- and long-range order of an isotropic material, can

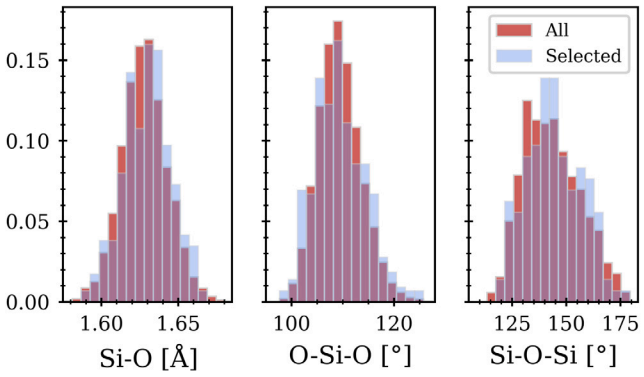

Fig. 3. Distributions of geometrical parameters of 20 amorphous SiO_2 structures created with molecular dynamics and cell optimized with density functional theory. The blue bins represent the parameters of the structure used for further defect calculations.

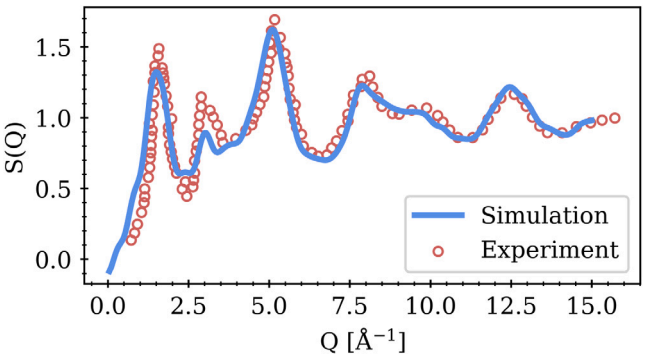

Fig. 4. Structure factor S as a function of the scattering vector Q of the structure used for defect calculations compared to S from neutron scattering experiments [55]. The location of the peaks is in excellent agreement for the whole Q range.

be extracted by X-ray and neutron diffraction experiments as a function of the scattering vector Q. The comparison of S of our structure to experimental neutron scattering data in SiO_2 [55] is shown in Fig. 4. S shows good agreement over the entire Q-range. Based on these structural agreements to experiments, we conclude that our final SiO_2 models are a reasonable representation of real a-SiO_2.

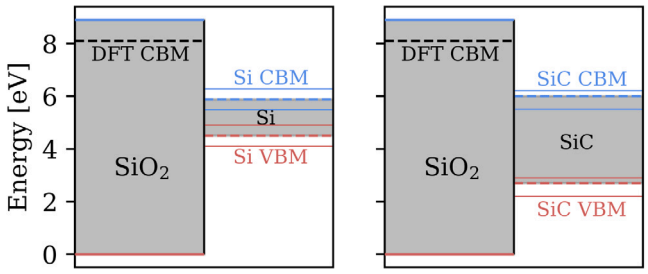

Fig. 5. Band diagrams of Si/SiO_2 (left) and SiC/SiO_2 (right) systems with an estimated tolerance of the band alignments schematically shown as colored bars according to differing literature values and DFT band gap corrections. Experimental values are shown as solid lines, dashed black lines are values calculated with DFT, dashed colored lines denote the energies of the band edges used in this work to investigate the interaction with defect levels.

2.4. Energy alignment

One major problem when comparing DFT results to experiment is the uncertainty in the energy offsets. Literature values of the VBM band offset of SiO_2 and Si from spectroscopy experiments are in the range of 4.3 to 4.7 eV [56–58], depending on the measurement techniques used and the sample growth conditions. In the following, we set the Si/SiO_2 VBM band offset to 4.5 eV for all calculations involving the electronic structure. The crystalline silicon (c-Si) band gap was calculated using our standard DFT setup and is slightly overestimated to 1.38 eV while the SiO_2 band gap was underestimated to 8.1 eV compared to the well-known values (1.1 eV for Si and 8.9 eV for SiO_2). The discrepancy to measured band gaps of Si crystals and SiO_2 oxides is caused by the employment of the PBE0_TC_LRC hybrid functional for our calculations, which tends to systematically overestimate band gaps of semiconductors and underestimate band gaps of insulators [59]. For the SiC/SiO_2 system, experimental and DFT values for the VBM band offset range from 2.2 to 2.9 eV above the SiO_2 VBM [60–62], depending on the processing and annealing condition and the orientation of the interface. Based on these various literature values, we set the VBM offset to 2.7 eV with a band gap of 3.3 eV for 4H-SiC [62] in the following. When discussing the interaction of calculated oxide defect levels with the band gap of a substrate, the before-mentioned corrections and resulting uncertainties of the presented energies always have to be considered. This uncertainty is schematically depicted as a colored tolerance bar of ±0.4 eV around the band edges in Fig. 5. For the sake of simplicity, we will only show the defect properties calculated with DFT without any error bars in the following.

3. Results

Here we analyze the three defect types OV, HB and H-E' and show a statistical analysis of their formation energies, relaxation energies, energy barriers and charge transition levels to validate a generalized multi-state defect model. The transitions between stable and metastable defect configurations are studied by calculating corresponding energy barriers. Furthermore, E_{Relax} and CTL are used to model the potential energy curves of the defects and to estimate energy barriers for charge transitions based on the harmonic potential energy surface approximation. We finally show correlations between defect properties and structural parameters of the corresponding precursor site. Recently, the impact of oxide defect properties like CTL, E_{Relax} and the defects distance to the interface were discussed and linked to charge trapping processes in SiC MOSFETs [20] for different temperatures and gate voltages and to time dependent defect spectroscopy (TDDS) [8] experiments in pMOSFETs for hole traps [63] according to the NMP model.

Table 1
Mean and standard deviation of characteristic distances (Si–Si for the OV, Si–H for the HB and Si–O for the H-E') of relaxed unpuckered defects OV (N = 124), HB (N = 131) and H-E' (N = 92) in different charge states.

Defect:	$q = 0$ [Å]	$q = +1$ [Å]	$q = -1$ [Å]
OV:	2.43 ± 0.09	2.93 ± 0.21/4.27 ± 0.33	2.60 ± 0.28
HB:	1.46 ± 0.01	1.59 ± 0.08	1.46 ± 0.04
H-E':	1.61 ± 0.01	1.77 ± 0.03	1.61 ± 0.04

3.1. Defect types

In the following, the three analyzed defect types OV, HB and H-E' are discussed for the three charge states q = 0, +1 and −1. The defects are shown for these charge states with their electron distribution around the defect site at an isovalue of 0.05 e/Å^3. Initial structures comprising one OV were created by removing a single oxygen within the cell. For the HB, an oxygen atom was replaced by a hydrogen atom. The hydroxyl-E' center defects were created by placing a hydrogen in the direct vicinity of a bridging O atom at a distance of 1 Å. For all defects, the geometry of the structures was optimized by DFT. First, the positively charged entity of the initial defect configuration was calculated. The resulting structure was subsequently used as a starting point for a geometry optimization in the neutral charge state, followed by a relaxation in the negative charge state. These procedures were repeated for all 144 oxygen sites in the structure to create 144 different initial defect configurations of each defect type in different charge states. For all three kinds, a number of initial defects spontaneously relaxed to puckered configurations [12], where a silicon atom moves through the plane of its three adjacent oxygen atoms, sometimes backbonding to another O atom. These configurations correspond for example to states 1′, 2 and 3 of the HB as shown in Fig. 1. Additional puckered configurations were created by forcing a relaxed defect structure to a puckered configuration and subsequently relaxing it with our DFT setup.

3.1.1. Oxygen vacancy

An OV for charge states q = 0, −1 and +1 is shown with its lowest unoccupied molecular orbital (LUMO) (positively charged) or its highest occupied molecular orbital (HOMO) (neutral and negatively charged) localized at the defect site in Fig. 6(a–c). In the neutral state (a), the HOMO is shared between the two silicon atoms to form the so-called dimer configuration, whereas in the positive charge state (b) the electron is localized on a single Si atom and forms a Si dangling bond. This configuration is known as a paramagnetic E' center and is the most common dangling bond in a-SiO_2 [15,16]. In addition to the Si–Si bond in the neutral charge state, this electron is shared almost equally within an anti-bonding orbital between the two Si atoms [64]. For the negatively charged OV, the respective HOMO is localized at both adjacent Si atoms. From the numerous possible configurations with a missing oxygen as discussed in [39], only the dimer (or unpuckered) and the puckered configuration, which account for more than 95% of all relaxed defects, will be analyzed in this work to allow for efficient characterization of the defect parameters. The average Si–Si distances of the relaxed OVs including the standard deviation are shown in Table 1. For q = +1, two different unpuckered defect configurations were found. First, one of the silicon atoms has a dangling bond (Si–Si distance of 4.27 ± 0.33 Å, 37 of all relaxed defects) and the second where the electron is shared between two silicon atoms similar to the neutral dimer configuration (Si–Si distance of 2.93 ± 0.21 Å). Most of the positively charged puckered OVs are lowered in energy when a Si atom finds an O in its vicinity where it can backbond to. The charge trapping properties of puckered and unpuckered OVs have also been studied across Si/SiO_2 and $Si/SiO_2/HfO_2$ interfaces in [65,66].

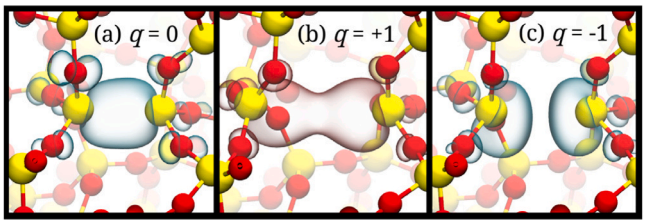

Fig. 6. Example of an unpuckered oxygen vacancy in different charge states with the respective highest occupied molecular orbital (HOMO) (blue) shown for the neutral (left) and negative (right) charge state and the lowest unoccupied molecular orbital LUMO (red) for the positive charge state (middle) at an isovalue of 0.05 e/Å^3.

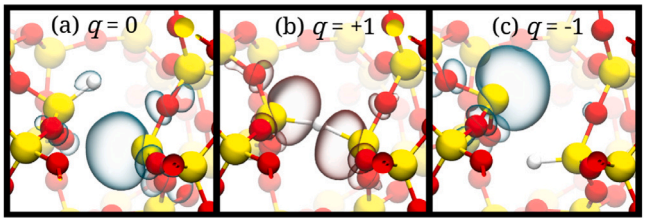

Fig. 7. An example hydrogen bridge in different charge states with its highest occupied molecular orbital (HOMO) (blue) or lowest unoccupied molecular orbital (LUMO) (red) at an isovalue of 0.05 e/Å^3. Charge states from left to right: neutral, positive, negative.

3.1.2. Hydrogen bridge

A hydrogen bridge can form when a hydrogen atom moves into a preexisting oxygen vacancy [36,67]. A typical HB in three charge states is shown in Fig. 7(a–c) with its HOMO in neutral and negative and its LUMO in positive charge state localized at the defect site. For $q = 0$ and $q = -1$, the hydrogen atom is bonded to one of the two silicon atoms, whereas for the positive charge state the resulting H is nearly centered between. The average Si–H bond lengths for the unpuckered configurations are shown in Table 1 for all three charge states. Similar to the OV, a positively charged puckered configuration is lowered in energy when backbonded to a fourth O atom.

3.1.3. Hydroxyl-E' Center

A hydroxyl-E' center forms, when a hydrogen atom gets attached to an O while breaking an elongated Si–O bond [22] and thereby forms a hydroxyl group. The H atom is then bound to an O atom with an adjacent dangling bond at a threefold-coordinated Si atom. An example of a typical H-E' is shown in Fig. 8 in the neutral (a) and positive charge state (b). Most of the 144 initial configurations with a hydrogen close to a bridging oxygen relaxed into a H-E' center in the neutral charge state, while 5% reconfigured into a geometrically similar but metastable defect, the so-called $[SiO_4/H]^0$ centers [22]. Both Si–O bonds are still intact for these unstable configurations but highly strained to ≥ 1.7 Å. For $q = +1$, the oxygen remains attached to both silicon atoms. The mean and the standard deviation of the Si–O bond lengths of the unpuckered H-E' are shown in Table 1 for all three charge states.

Negative charge state:. Several different configurations were found for the H-E' center in the negative charge state with four of them shown in Fig. 8(c–f). The most stable configuration consists of an intact Si–O bond with the H getting attached to a nearby Si atom making it fivefold coordinated (f) [67,68]. This configuration is on average 1.5 eV lower in total energy compared to configurations where the Si–O is broken similar to the neutral and positive charge state (c–d) or the oxygen vacancy like configuration (e). Occasionally, these states can also have puckered configurations, which are generally even higher in energy as shown in Section 3.3.1 and will therefore be omitted. Energy barriers for transitions to the stable configuration were calculated with

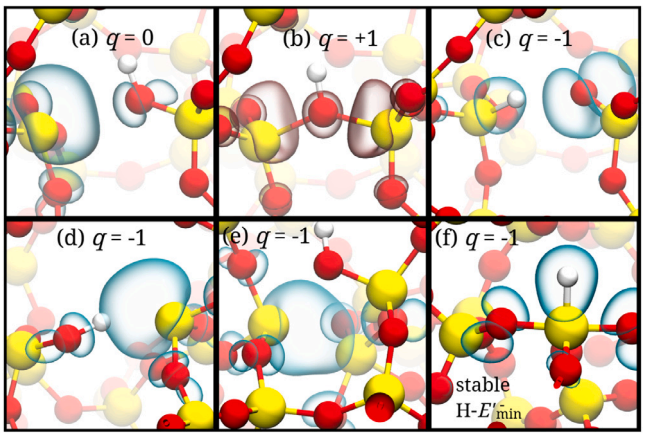

Fig. 8. Hydroxyl-E' center in different charge states with its highest occupied molecular orbital (HOMO) (blue) or lowest unoccupied molecular orbital (LUMO) (red) at an isovalue of 0.05 e/Å^3. Charge states: neutral (a), positive (b), negative metastable (c–e) and the minimum energy configuration of the negatively charged hydroxyl-E' center (f).

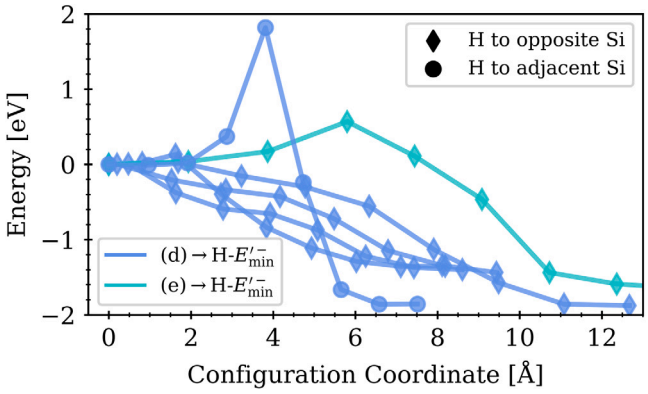

Fig. 9. Transition barriers from metastable negatively charged H-E' configuration to the H-E'^{-}_{min} configuration (equivalent to the $3' \rightarrow 3$ transition in the state diagram in Fig. 1). Energies of the metastable H-E' configurations are set to arbitrary 0 eV and correspond to the configurations shown in Fig. 8 as denoted in the legend while the marker denotes the Si position where the H moved to.

CI-NEB and are presented in Fig. 9. Depending on the configuration, the defect relaxes into the minimum energy configuration with almost no barrier (<0.05 eV) with the H moving to the Si opposite the hydroxyl group while the barrier for an attachment of H to the adjacent Si is rather large (>1.8 eV) for the calculated site. After trapping an electron (similar to $1 \rightarrow 3'$ in Fig. 1), the defect is expected to briefly stay in one of these configurations before the O is bound to the Si atoms again and H gets attached to one of the Si ($3' \rightarrow 3$). Due to the small transition barriers and comparably high total energies, we consider configurations (c-e) to be local minima of the PEC and thus metastable. The minimum configuration will be referred to as H-E'^{-}_{min} in the following. Upon the release of an electron, the hydrogen was often found to become interstitial and consecutively creates a defect, potentially at a different position in the oxide ($3 \rightarrow 0$ vs. $3 \rightarrow 1$).

3.2. Formation energy

The formation energy E^q_{Form} of a defect in charge state q is given by

$$E^q_{\mathrm{Form}} = E^q_{\mathrm{tot}} - E^{\mathrm{bulk}}_{\mathrm{tot}} - \sum_i \mu_i n_i + q E_{\mathrm{F}} + E^{\mathrm{corr}} \quad (1)$$

where E^q_{tot} is the total energy of the system with the defect in charge state q, $E^{\mathrm{bulk}}_{\mathrm{tot}}$ is the total energy of the defect-free neutral bulk, $\mu_i n_i$

stands for the chemical energy needed to add or remove atoms of kind i to the bulk to create the defect. The Fermi level E_F is calculated relative to the valence band maximum of the oxide $E_F = E_{VBM} + \epsilon_F$, where E_{VBM} can be approximated by the highest occupied Kohn–Sham orbital of the defect free-bulk system [69]. The correction term E^{corr} is needed for DFT calculations of charged systems with periodic boundary conditions to remove spurious interactions with image charges. The correction term was calculated with

$$E^{corr} = \frac{q^2 \alpha_M}{2\epsilon L} \tag{2}$$

which corresponds to the Madelung term in the image charge correction scheme of Makov and Payne [70], Here, α_M is lattice-dependent Madelung constant, ϵ is the static dielectric constant and $L = V_{SC}^{-1/3}$ is the supercell dimension of volume V_{SC}. E^{corr} was calculated to ≈0.35 eV for every charged defect. This simple correction was compared to a numerical energy correction scheme [71], where the electrostatic potential calculated with DFT is compared to an ideal point charge in the system. Subsequently, both potentials are aligned which yields the correction value. The E^{corr} of this scheme for 5 random defects differed by less than ±0.03 eV compared to the one of Makov and Payne. We therefore justify setting $E^{corr} = 0.35$ eV for every charged defect.

The formation energies E_{Form} of the neutral defects are shown in Fig. 10. For all defect types, the extracted parameters of the distributions are given in the plot. Formation energies for oxygen vacancies are given with respect to the pristine bulk system. This reference makes the total values arbitrary as in reality OVs are mostly introduced in SiO_2 during oxidization, but occasionally can also be created in the vicinity of already existing OVs during an applied bias [72]. Furthermore, we approximate the chemical potentials used in Eq. (2) with the total energies obtained with our DFT setup, half the energy of an H_2 molecule for μ_H and half the energy of an O_2 molecule for μ_O. As can be seen in Fig. 10 (top), puckered OV configurations have a significantly higher formation energy than the unpuckered configurations. The accumulated formation energies of the OV defects can both be described by a normal distribution, the fitting parameters are shown in the figure.

For the hydrogen bridge defects, the formation energies are given with respect to their precursor configuration (unpuckered and puckered OVs respectively) in Fig. 10(b), which is assumed to be the oxygen vacancy at the respective defect site. Furthermore, in Fig. 10(c), E_{Form} of HB defects is also given with respect to the perfect bulk system to compare the formation energies of the two hydrogen related defect types. Since in the case of the unpuckered HB the distribution of the formation energies is asymmetrically shifted to higher values, as can be seen in Fig. 10(b), a Weibull distribution was chosen here for the most suitable fit which is given by Eq. (A.1) shown in the Appendix. Puckered HB configurations tendentiously posses a lower E_{Form}. For the majority of the HB defects (61.5%), the formation energy is negative when referencing to an already existing OV, indicating that the HB is actually the preferred defect configuration in this case. Nevertheless, due to the extremely high formation energy of the HB in a perfect bulk system, the creation of hydrogen bridges is limited by the already low concentration of oxygen vacancies ($10^{14} - 10^{18}$ cm^{-3}) in a-SiO_2 thin films [6,73,74].

The formation energies of the last investigated defect, the H-E', are again given with respect to the bulk system. Compared to the two other defect types, E_{Form} gives feasible concentrations for H-E' defects only limited by the number of hydrogen atoms in the oxide (10^{20}–10^{22} cm^{-3}) [75,76]. Defects with formation energies >4.5 eV were all identified as $[SiO_4/H]^0$ defects. These configurations are metastable with a similar energy compared to H being interstitial and with only a small barrier to relax to a H-E' as it was shown in [22]. Because they are unlikely to form naturally compared to the H-E' centers, they are excluded from the normal distribution fit and will not be analyzed in the further discussions.

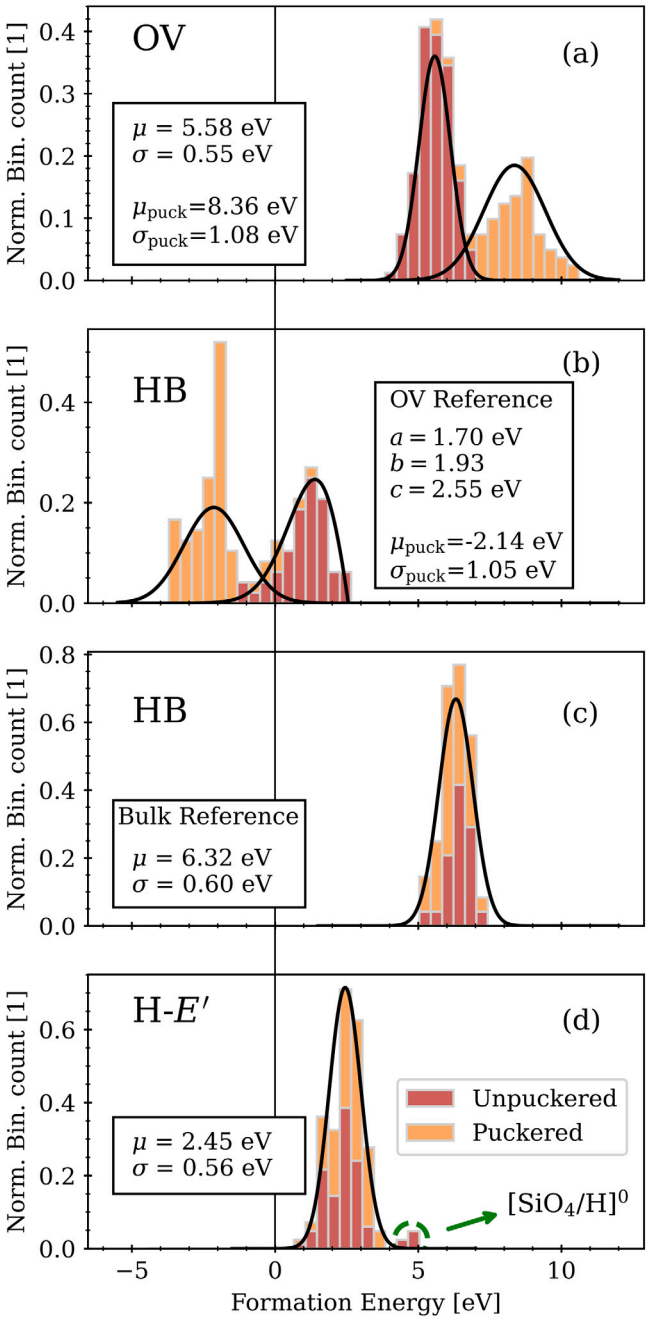

Fig. 10. Distributions of formation energies for unpuckered and puckered defects of type OV, HB and H-E'. E_{Form} of HB defects were calculated with the corresponding OV and the pristine bulk system as reference. Normal and Weibull distribution (HB unpuckered with OV reference) fits were made to distinguish peaks of the formation energies of each defect type.

3.3. Transitions without charge transfer

In this section, the metastable defect configurations, which correspond to the states denoted with a prime in Fig. 1 and the local minima in Fig. 2, are analyzed in terms of their relative energy and activation barriers with respect to the stable configuration.

3.3.1. Metastable configurations

The three investigated defect types can also all exist in puckered configurations in all charge states as described in Section 3 and shown for a HB in Fig. 1. Some of the puckered defects formed spontaneously

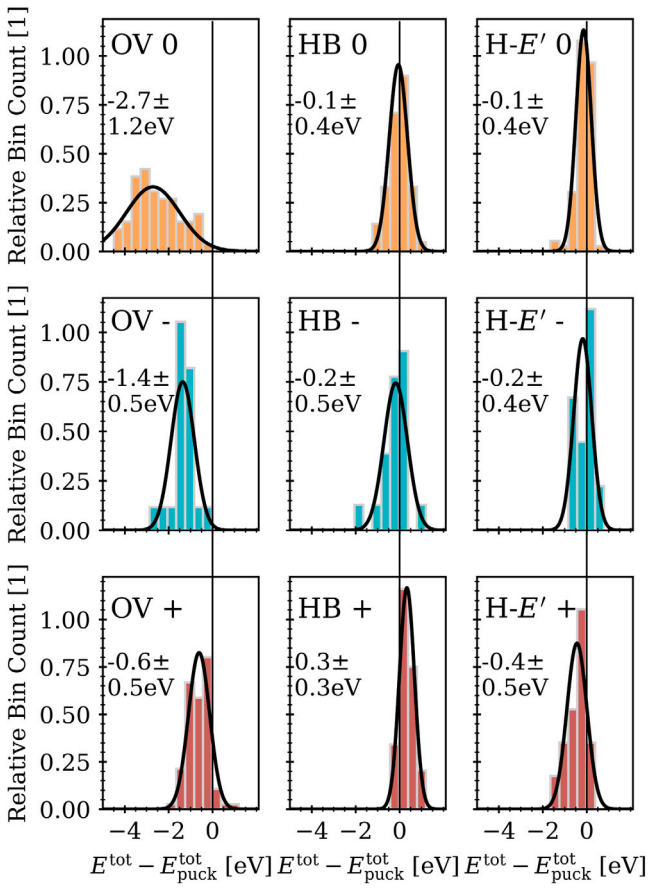

Fig. 11. Total energy differences between unpuckered and puckered configurations of oxygen vacancies (left), hydrogen bridges (middle) and hydroxyl-E' centers (right) in the neutral (top), negative (middle) and positive (bottom) charge state.

during relaxation, while the remaining initial puckered configurations were intentionally perturbed by moving the central Si atom through its plane of the backbonded O atoms in order to deliberately create such a state. The energy differences between puckered and unpuckered configurations in the respective neutral, negative and positive charge states are shown in Fig. 11. Normal distributions were fitted to the energy differences with the parameters given in the plot. The unpuckered OV is clearly the preferred configuration with substantially lower energies. For the hydrogen related defects, HB and H-E', both the puckered and the unpuckered can be the configuration lower in energy, depending on the respective atomic surroundings of a certain defect. The transition barriers between these two configurations are discussed in the following.

3.3.2. Transition barriers

Transition barriers between puckered and unpuckered configurations for all three defect types in the negative charge state were calculated using the CI-NEB method. Barriers for positively charged and neutral defects have been already reported in [12]. Due to the enormous amount of core hours needed for such calculations ($>10^4$ h), only a small number (<10) of barriers for each transition could be carried out. The results are shown in Fig. 12. For OV and HB defects, these barriers correspond to the $3 \leftrightarrow 3'$ transition. For the H-E', these calculations are a bit artificial as the unpuckered configurations (Fig. 8(c-e)) are already highly unstable and rapidly relax into the H-E'^{-}_{min} configuration as shown in Section 3.1.3. In Fig. 12 (left), three different energy profiles are plotted as a function of the configuration coordinate (left) to show the variety of the possible transitions. The

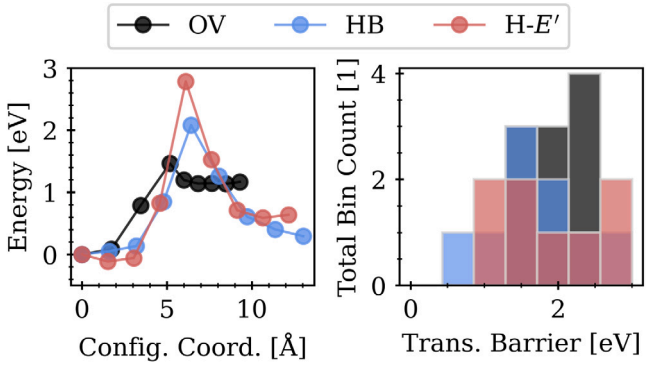

Fig. 12. Typical energy profiles for the charge conserving transitions between stable and metastable negatively charged states of the three defect types as a function of the configuration coordinate (left). The energy barriers for the transition from stable to metastable states are shown on the right side.

energy barriers for the transition from the stable to the metastable state are shown in Fig. 12 (right). Barriers vary from 1.5 to 2.5 eV (OV), 0.8 to 2.7 eV (HB) and 0.95 to 2.9 eV (H-E'). The broad range of activation energies for these thermal transitions can be directly linked to the different timescales of defects staying electrically inactive (ps to years [14]).

3.4. Charge transition level

The charge transition level (CTL) corresponds to the Fermi level E_F at which the formation energies (Eq. (2)) of a defect in two different charge states are equal. In other words, the thermodynamically preferred charge state of the defect depends on the relative position of its trap level to the Fermi level. When a defect traps a charge, the localization of the electron in the oxide disturbs the electrostatics of the device, which alters important device properties like the threshold voltage [11,20]. The CTL is the only defect parameter which is directly accessible through electrical experiments. By applying a gate bias to a MOS device, the position of the trap level can be shifted due to band bending near the interface and the occurring electric field in the oxide. When the Fermi level matches the CTL, both involved charge states are equally stable resulting in equal occupancy and maximum power of the RTN signal [77]. In principle, the CTL of a defect is an inherent property of the host material, e.g. the oxide of a MOSFET, independent of the electronic bands of a potential substrate. With that being said, the morphology of the interface to the substrate can influence the CTL indirectly via strain or changes in the stoichiometry. Furthermore, the interfacial environment could give rise to entirely new defects not present in the bulk oxide. However, an in-depth treatment of these effects is beyond the scope of the present work and should be investigated separately in the future.

CTLs were calculated for all possible transitions depicted in Fig. 2. Following the commonly employed band edge approximation [19], interaction of defects is limited to the band edges of the Si substrate, as illustrated with arrows in the shown state diagrams. Note that the uncertainties of band alignments and energy values obtained from DFT calculations as discussed in Section 2.4 have to be considered when analyzing CTLs in the context of a band diagram. Only defects where the electron is fully localized at the defect site for both charge states are considered for the calculations. Not all defects converged into both stable puckered and unpuckered configurations in every charge state, limiting the possible charge transitions, e.g. the hole trapping mechanism from a 4-state defect $1 \leftrightarrow 1' \leftrightarrow 2 \leftrightarrow 2' \leftrightarrow 1$ to a 3-state $1' \leftrightarrow 1 \leftrightarrow 2'$ or a 2-state $1 \leftrightarrow 2'$ defect . This is for instance the case when the Si of a positively charged H-E' defect has no fourth O in its atomic environment to backbond to, meaning that no stable puckered

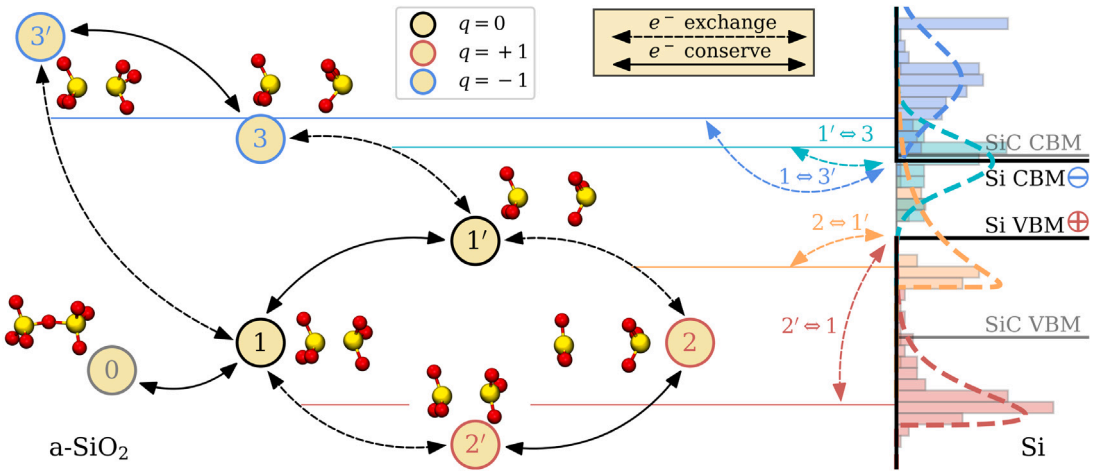

Fig. 13. State diagram of an oxygen vacancies with their distributions of charge transition levels shown in the context of a Si/SiO_2 (black) and a SiC/SiO_2 (gray) band diagram. CTLs are fitted with either a normal or a Weibull distribution with the extracted parameters given in Table 2.

Table 2
Fitting parameters for charge transition levels of oxygen vacancies, hydrogen bridges and hydroxyl-E' centers (normal and Weibull-distributions) relative to $E_V(SiO_2)$. The band offsets of Si/SiO_2 and SiC/SiO_2 systems and their tolerances are discussed in Section 2.4.

Normal distribution			
Defect	Transition	μ [eV]	σ [eV]
OV	$1 \leftrightarrow 3'$	7.38	0.67
	$1' \leftrightarrow 3$	5.89	0.46
HB	$1 \leftrightarrow 2'$	4.35	0.50
	$1 \leftrightarrow 3'$	5.72	0.45
	$1' \leftrightarrow 3$	5.94	0.66
H-E'	$1 \leftrightarrow 2'$	5.08	0.52
	$1' \leftrightarrow 2$	4.94	0.50
	$1 \leftrightarrow 3'$	5.70	0.29
	$1 \leftrightarrow 3$	4.24	0.42

Weibull distribution				
Defect	Transition	Loc c [eV]	Shape b [eV]	Scale a
OV	$1 \leftrightarrow 2'$	1.10	1.26	0.63
	$1' \leftrightarrow 2$	3.61	0.87	1.05
HB	$1' \leftrightarrow 2$	3.60	1.10	1.05

configuration (2) exists at this defect site. The actual number of n-state defects cannot be sufficiently determined via our path, as it is quite difficult to verify if a certain configuration really does not exist or if the defect system only relaxed to a different local minimum during the DFT geometry optimizations due to an insufficient starting point. Hence, we show all possible CTLs in a normalized histogram for all calculated transitions in the following, regardless the number of stable states of a certain defect. The correlations of trap levels of 4-state defects will be further analyzed in Section 3.6. The CTL data is plotted in the context of a Si/SiO_2 and a Si/SiC band diagram (see Section 2.4) with the corresponding atomic configurations for a respective charge transition shown on the left side for each defect type.

3.4.1. Oxygen vacancy

The CTLs of oxygen vacancies for both charge transitions and all three defect configurations are shown in Fig. 13. Although OVs are generally introduced in the system during oxidization, a precursor configuration (0) is shown in the figure, as it has been suggested that an OV can also be generated near an already existing OV or near a wide O–Si–O angle when two electrons are trapped at these sites [72]. The majority of the $1 \leftrightarrow 2'$ transitions lie far below the Si valence band maximum while the $1' \leftrightarrow 2$ have substantially higher CTLs. OVs can therefore capture a hole mostly via the $1' \leftrightarrow 2$ transition, which requires the positively charged OV to be in the puckered configuration corresponding to the E'_γ center [39]. When the defect relaxes to the $2'$ state, the subsequent CTL $1 \leftrightarrow 2'$ lies energetically too low to exchange charge carriers with the VBM of Si. This process could explain disappearing defects or anomalous random telegraph noise (RTN) as reported in [78]. Furthermore, the low CTLs of OVs could give an explanation for BTI also reported in Si/SiC devices [20]. The $1 \leftrightarrow 2'$ and $1' \leftrightarrow 2$ transitions of the OV are asymmetrically distributed due to the two configurations of the positively charged OV (see Section 3.1.1) and were therefore fitted with a Weibull distribution (Eq. (A.1)) with the fitting parameters given in Table 2. This asymmetry is due to sporadically occurring OV configurations in the positive charge state that relatively lower the total energy of the defect system, namely puckered OVs with a backbonded Si atom as already discussed in Section 3.1.1. Hence, we confirm, that in a MOSFET during normal operation, it is unlikely for an OV to exchange charge carriers with the Si substrate in ultra-scaled devices [12,17,18,67]. Still, the +/0 CTLs of OVs are in a reasonable energy range to trap holes from the VBM of a SiC substrate. For the −/0 transitions on the other hand, a portion of the $1' \leftrightarrow 3$ and the $1 \leftrightarrow 3'$ CTLs are in the vicinity of the Si and SiC CBM and thus OVs have to be considered as a possible cause for electron capture events during operation. The total effect of OV on BTI is limited by the low number of oxygen vacancies in a-SiO_2 as discussed in Section 3.2. It should be noted that the OV is also stable in charge state (2+), which might be of interest for future investigations concerning the hole trapping behavior in SiO_2/SiC systems.

3.4.2. Hydrogen bridge

For the two defect types involving H the situation is completely different. The charge transition levels are shown in Fig. 14 with their corresponding atomic configurations on the left side. The asymmetric distribution of the $2 \leftrightarrow 1'$ CTLs can be explained by backbonded puckered HB defects in the positive charge state occurring at certain sites in the structure (see Section 3.1.2). Similar to the OV defects, these backbonded HBs are lower in energy compared to defects where no fourth O for backbonding is nearby in the structure. Fitting parameters for normal and Weibull distributions for all transitions are again given in Table 2. In contrast to the OV, the majority of the HB defects possess trap levels close to the band edges of the Si substrate, which would make them promising defect candidates to explain reliability degrading phenomena induced by electron as well as hole trapping. Nevertheless, as discussed in Section 3.2, the concentration of HBs is strongly limited by the number of OVs in the oxide. The high formation energies of HBs in a vacancy free bulk system limit their concentration and thus the influence of this defect type on reliability phenomena is likely negligible.

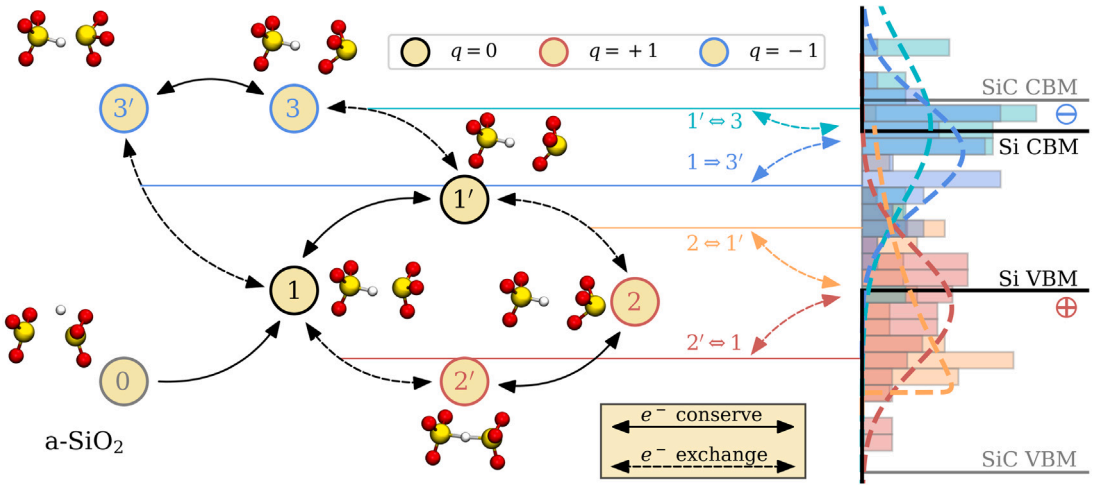

Fig. 14. State diagram of a hydrogen bridge in three charge states with the calculated charge transition level distributions shown in the context of a Si/SiO_2 and a SiO_2/SiC band diagram. CTLs are fitted with either a normal or a Weibull distribution with the extracted parameters given in Table 2.

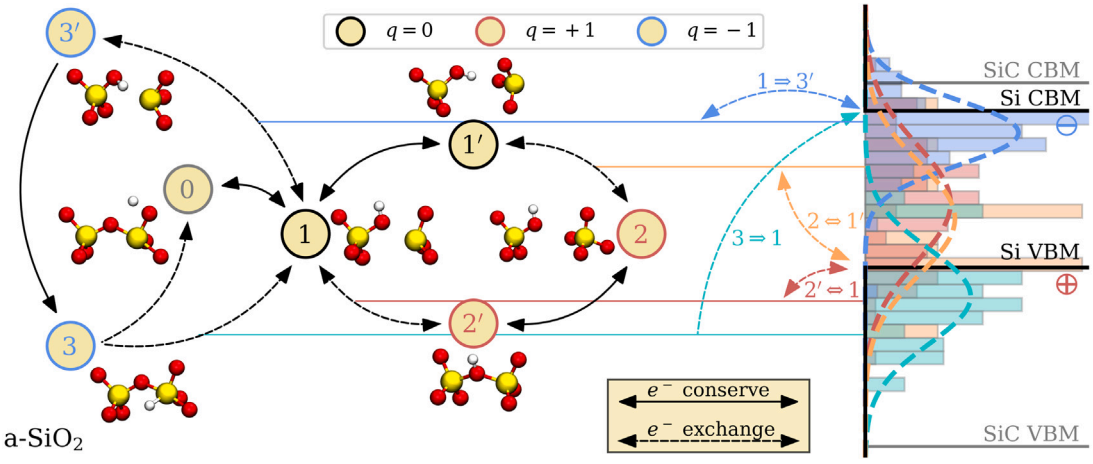

Fig. 15. State diagram of a hydroxyl-E' center with the calculated charge transition level distribution shown in the context of a Si/SiO_2 and a SiO_2/SiC band diagram. CTLs are all fitted with a normal distribution with the extracted parameters given in Table 2.

3.4.3. Hydroxyl-E'

The state diagram of H-E' defects with their according CTLs are shown in Fig. 15. For the CTLs of the H-E' defect, both +/0 trap levels of H-E' are distributed across the VBM of Si which makes them reasonable defect candidates for trapping holes from the substrate. CTLs for all transitions were fitted with a normal distribution with the fitting parameters given in Table 2. The $1 \leftrightarrow 3'$ CTLs near the conduction band edge correspond to the negatively charged metastable H-E' configurations shown in Fig. 8. Additionally, the $1 \leftrightarrow 3$ CTLs near the VBM of silicon correspond to defects with the H-E' $^{-}_{\text{min}}$ configuration in the negative charge state. As all other negatively charged H-E' configurations, puckered or unpuckered, rapidly relax into this minimum configuration as shown in Fig. 9, we argue that mainly CTLs corresponding to the negatively charged minimum configuration are detectable in real oxides. Note that the neutral level in this transition can also correspond to the $1'$ state, depending on the atomic environment. Compared to the hole trapping mechanism, the $3 \rightarrow 1$ CTLs of the H-E' are energetically farther away from the respective charge reservoir, which reduces the total amount of charge trapping defects in the oxide, thus providing a sensible explanation for the suppressed electron trapping behavior observed in Si/SiO_2 MOS devices.

3.5. Charge transition barriers

In this section, the PECs of H-E' defects in the harmonic approximation are constructed by fitting a parabola to the equilibrium and relaxation energies of the defects in different charge states. The energy barriers for all single charge capture and emission processes shown as stars in Fig. 2 are subsequently extracted from the crossing points of the PECs. We show that the −/0 (+/0) transition is energetically always favorable compared to the −/+ (+/−) transition.

3.5.1. Relaxation energy

Relaxation energies give information about the shape of potential energy surfaces in different defect charge states, in particular the curvature near the energy minimum, as shown in Fig. 2. Within the frequently employed harmonic approximation, the crossing point and hence the classical barrier between two differently charged PEC of a defect is completely determined by the relaxation energies and the trap level. Therefore, E_{Relax} heavily influences the resulting capture and emission time constants of the defect [14]. When the charge state changes from 0 to −1 (+1), the relaxation energy will be denoted in the following as $E^{0/-}_{\text{Relax}}$ ($E^{0/+}_{\text{Relax}}$) and vice versa $E^{-/0}_{\text{Relax}}$ ($E^{+/0}_{\text{Relax}}$). To calculate the relaxation energies for each possible charge transition, single point calculations were carried out on relaxed defects in opposite charge

Table 3
Normal distribution fitting parameters for relaxation energies of oxygen vacancies, hydrogen bridges and hydroxyl-E' centers. E_{Relax} of OVs including a positive charge state follow a bimodal distribution.

Relaxation energies			
Defect type	Transition	Mean [eV]	Std. Dev. [eV]
OV	0/−	1.18	0.34
	0/+	1.5/2.53	0.17/0.36
	−/0	1.78	0.25
	+/0	2.25/3.5	0.18/0.42
HB	0/−	1.72	0.42
	0/+	2.20	0.17/0.29
	−/0	1.76	0.41
	+/0	2.21	0.36
H-E'	0/−	1.97	0.28
	0/+	2.98	0.32
	−/0	1.59	0.1
	+/0	2.4	0.45
	+/−	13.14	0.21
	−/+	7.87	0.9

states. The relaxation energy for the transition 0/− for example can then be simply calculated as the energy difference to the relaxed defect in the same charge state

$$E^{0/-}_{\mathrm{Relax}} = V^{-}(Q_1) - V^{-}(Q_3) \tag{3}$$

where Q_1 and Q_3 are the equilibrium positions of the defect configuration in charge state 0 and −, respectively, as shown in Fig. 2 (right). Thus, E_{Relax} can also be interpreted as the amount of energy being transferred from the defect to the thermal bath after a radiative charge transfer. In the nonradiative case, the relaxation energies are a measure for the classical barrier of the charge transfer. Relaxation energies for each defect type are presented in Table 3. A small number of single point calculations did not meet the convergence criteria for some charged defects, as these calculations are performed on unrelaxed structures. Most of the relaxation energies for all defect types and possible charge transitions are distributed between 1 and 4 eV. The relaxation energies for charge transitions from or to the negative charge state tend to be lower in energy for most of the defects, with the majority (≈ 75 %) below 2 eV (100% for $E^{0/-}_{\mathrm{Relax}}$ of the OV) . For the +/0 and 0/+ transition of the OV and HB two peaks are visible. This is due to the two different OV configurations in the positive charge state as described in Section 3.1. Relaxation energies between negatively and positively charged defect states are significantly higher compared to the neutral/charged transitions which has a crucial impact on the charge transition barriers as will be shown in the following.

3.5.2. Potential energy curves

Parabolas were fitted to minimum and relaxation energies of H-E' defects to extract the transition barriers from the crossing point of two PEC. An example for the fitted PECs of an H-E' defect is shown in Fig. 16, where the parabolas are shifted as a function of the Fermi level according to Eq. (2) depending on the charge state. PECs are fitted for Fermi levels at the +/0 and −/0 CTLs (left and right) and for a Fermi level inside the band gap of Si (middle).

3.5.3. Charge transition barriers

The energy barriers extracted from the fitted PECs for 78 different H-E' defects are shown in Fig. 17 for Fermi levels at the VBM, inside the band gap and at the CBM of the Si substrate. For the −/0, 0/+ and −/+ transitions, the energy barriers become higher with increasing Fermi level while the opposite is true for 0/−, +/0 and +/− transitions. This behavior can directly be linked to the parabola and shift of the crossing point as seen in Fig. 16. We furthermore analyze which charge transition process is energetically favored by comparing the height of the transition barriers of two (q/0) and three ($-q/q$) particle processes

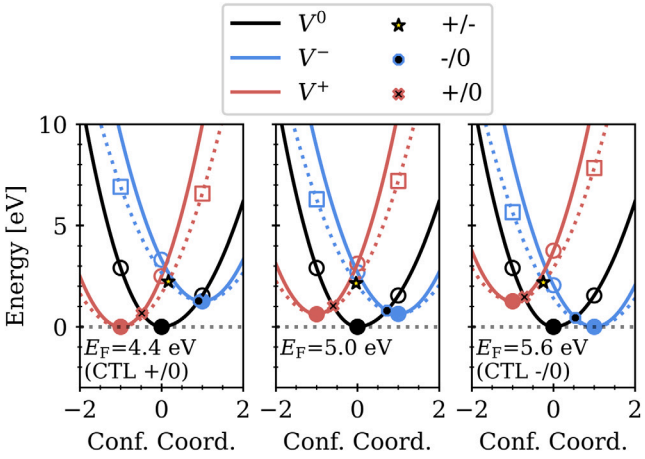

Fig. 16. Potential energy curves of a single H-E' defect in different charge states in the harmonic approximation obtained from parabolic fits to the equilibrium (full circles) and relaxation energies (empty circles for $0/q$ and squares for $-q/q$ transitions). PEC are shown from left to right as a function of the Fermi level (left at CTL for +/0, right at CTL for −/0 transition). The full lines denote fits with $E^{0/q}_{\mathrm{Relax}}$ while dotted lines are fitted to $E^{-q/q}_{\mathrm{Relax}}$. Transition barriers can be extracted from the crossing points of the barriers.

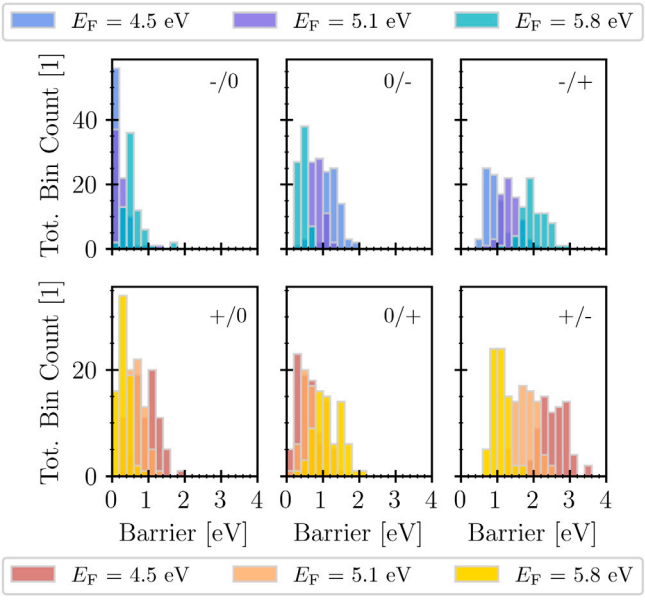

Fig. 17. Energy barriers for charge transitions at H-E' defect sites extracted from potential energy curves in the harmonic approximation for different Fermi levels according to Fig. 16.

by showing the energy difference between $-q/q$ and $q/0$ barriers in Fig. 18. For all 78 defects, the barrier for a $0/q$ charge transition is lower than for a transition involving two charge carriers for all investigated Fermi levels which makes them energetically far more favorable. Furthermore, processes involving three particles have a much smaller effective cross section, as the probability of three particles to collide becomes vanishingly low. Hence, we conclude that the transitions $3 \rightarrow 2'$ and $2 \leftrightarrow 3'$ are unlikely, though not completely impossible, to occur compared to processes where only one electron or holes is exchanged.

3.6. Defect correlations

In this section, correlations of certain defect properties are analyzed. We show how different charge transition levels (e.g. $1' \leftrightarrow 2$ and $1 \leftrightarrow 2'$)

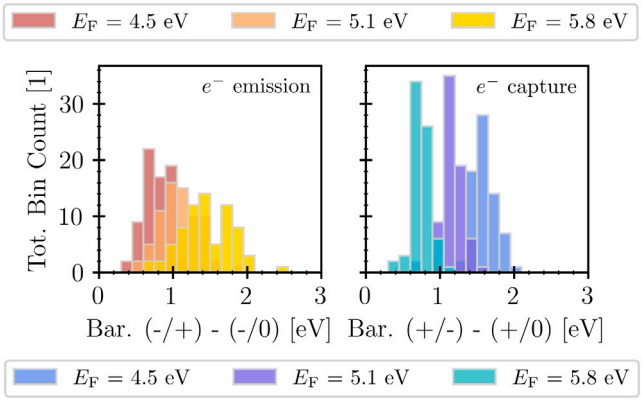

Fig. 18. Energy differences of transitions barriers between −/+ (+/−) and −/0 (+/0) charge transitions of 78 H-E' defects. Barriers for transitions involving two charge carriers are always higher.

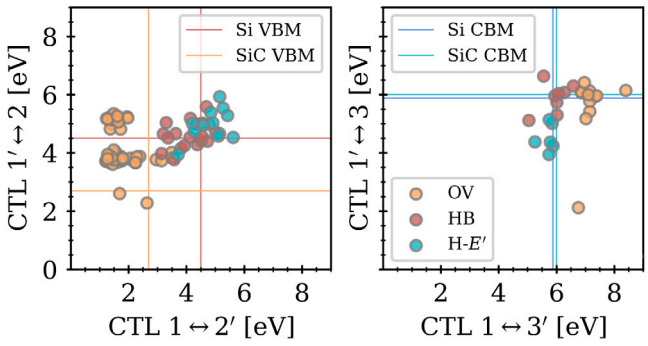

Fig. 19. 1′ ↔ 2 and 1 ↔ 2′ CTLs of single defects for capturing holes (left) and electrons (right) of OVs, HBs and H-E' centers plotted against each other. The relevant band edges Si and SiC substrates for the charge transfer are shown as colored lines.

of the same defect relate to each other. Furthermore, the dependence of CTLs on formation energies and the atomic environment of the defects is shown.

3.6.1. Transition levels

The correlation of different charge transition levels is depicted in Fig. 19. Each data point corresponds to one single defect, the relevant band edges of the Si bulk for charge exchange are drawn as red (VBM) and blue (CBM) lines, respectively. Only defects where all four configurations of Fig. 1 converged for each charge trapping mechanism are used for this analysis. The hole trapping levels are shown on the left side. For the OV, defects with the 1′ ↔ 2 CTL near the VBM of the substrate have very deep 1 ↔ 2′ levels. These deep levels can explain defects staying electrically inactive over a long time (months) after being charged according to the 1′ ↔ 2 transition. This effect can also be observed for the HB and H-E' defects but is weakened for this process due to the vicinity of the CTLs to the band edges and the more linear correlation of the transition levels. The relationship between the different electron capture levels is shown in Fig. 19 (right). For all three defect types, the 1 ↔ 3′ levels have no clear dependency on the 1′ ↔ 3 levels, but the CTLs of a single defect can also differ by more than 2 eV.

3.6.2. CTL and structural properties

In Figs. 13–15, the calculated CTLs are shown regardless of the probability that a certain defect will actually form. To analyze the plausibility of the occurrence of a certain CTL, a correlation plot of the formation energies and the 1 ↔ 2′ and 1 ↔ 3′ CTLs of the unpuckered defects was made in Fig. 20. The color gradient illustrates a characteristic geometrical quantity of the neutral precursor configuration for

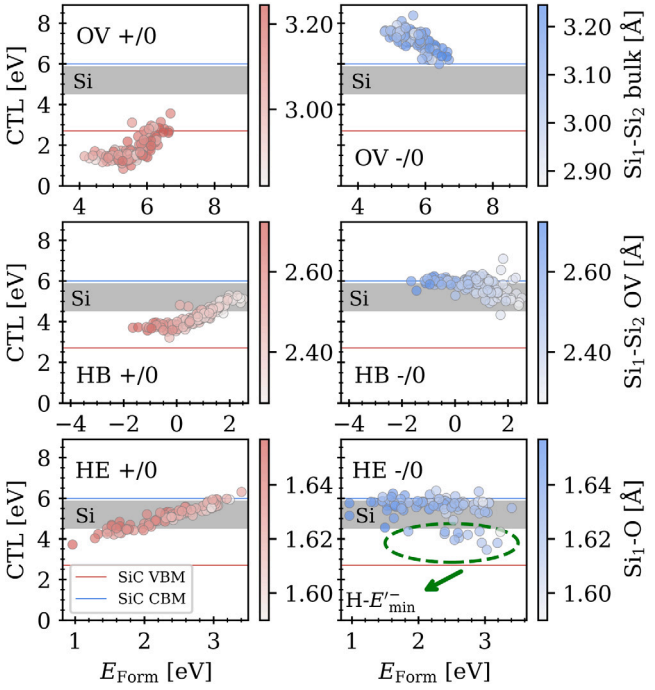

Fig. 20. Charge transition levels of unpuckered SiO_2 defects as a function of their formation energy. The color gradient represents specific geometrical distances of the precursor configuration of each defect.

each defect type: For OVs the distance of two silicon atoms before the oxygen atom between them was removed (Fig. 20 top), for the HB the distance between two silicon atoms of an OV before the hydrogen was captured (Fig. 20 middle) and for the H-E' the length of the two Si–O bonds before the bond was broken by a hydrogen getting attached to the O (Fig. 20 bottom). Oxygen vacancies which have their CTL closer to the band edges of the silicon substrate have comparably higher formation energies making their occurrence even less likely. Hydrogen bridges preferably form at prolonged Si–Si distances of an OV, as is indicated by the color gradient at lower formation energies in Fig. 20 (middle). The CTLs for the +/0 transition with the lowest formation energies are below the silicon VBM, while the CTLs in the middle of the band gap are less likely to form. HB 0/− transitions show a similar characteristic, where defects with the lowest E_{Form} have CTLs close to the CBM of the substrate while for higher formation energies the CTLs tend to be located within the Si band gap. We confirm that H-E' defects form preferably at strained Si–O bonds [21]. These are also the defects which have the highest chance to capture a hole from the Si substrate, as it is shown in Fig. 20 (bottom). The H-E' −/0 transitions show only weak dependency on the formation energy for both 1 ↔ 3′ and 1 ↔ 3 (denoted as configurations involving the H-E'^-_{min} configuration) and their CTLs are mostly independent of the corresponding E_{Form} and the Si–O bond lengths.

4. Discussion

We have investigated three major defect types in amorphous SiO_2, namely the oxygen vacancy (OV), the hydrogen bridge (HB) and the hydroxyl-E' center (H-E') and provided a large data set of their defect properties. By calculating the formation energies E_{Form}, the charge transition levels (CTLs), the relaxation energies E_{Relax} and the metastability of the defects, a multi-state defect model was developed to describe both electron and hole capture in a unified manner. Particular focus was put on the credibility of the utilized a-SiO_2 structures which were created using a melt and quench procedure and are in excellent

agreement with experimental perceptions. To account for the amorphous nature of SiO_2, we calculated a large ensemble of structural and electronic parameters of the aforementioned defects in different charge states on a statistical level.

Analogous to the already well investigated neutral and positively charged defects, we find negatively charged stable and metastable configurations where the additional electron localizes at the defect site. The negatively charged defect configuration were a H attaches to a Si making it fivefold coordinated was named H-E'^{-}_{min}, as all other discovered negatively charged H-E' proved to be metastable with almost vanishing energy barriers to relax to H-E'^{-}_{min}. Furthermore, energy barriers between puckered and unpuckered configurations in the negative and neutral charge state of all defect types were calculated with the climbing image nudged elastic band method (CI-NEB) and range from 0.8 to 3 eV. The metastable states and their according transitions to the stable configuration in the same charge state can explain the enormous range of time scales of point defects staying electrically inactive.

We show for all three defect types that both E_{Form} and CTLs for electron and hole capture are well represented by either a normal or a Weibull distribution. We confirm that the majority of the CTLs of OVs for hole capture processes are energetically too low with respect to the VBM of a Si substrate to interact with its charge carriers. Puckered OVs have CTLs distributed around 1 eV below the Si VBM. When a puckered OV traps a hole ($1' \leftrightarrow 2$) and relaxes to an unpuckered configuration ($2 \leftrightarrow 2'$), the according $2' \leftrightarrow 1$ CTL is energetically too low to exchange charge carriers with the VBM. This procedure may explain vanishing defects in irradiated oxides, where toggling signals caused by E' centers can be detected before the signals disappear as reported in [79].

Furthermore, we show that OVs have CTLs for hole trapping near the VBM of SiC substrates and could therefore be a cause for BTI observed in SiC/SiO_2 devices. Also, for the $-/0$ transition, OV defects can occasionally have CTLs which are close to the Si conduction band minimum ($1 \leftrightarrow 3'$) or inside the band gap of the Si substrate ($1' \leftrightarrow 3$), which would make them suitable defect candidates to capture electrons. Nevertheless, as a consequence of the small number of OVs in SiO_2, which is essentially determined by the highest oxidation temperature [80,81] due to its high formation energy in the SiO_2 bulk (5.6 ± 0.5 eV), the total influence of OVs on charge trapping processes is reduced compared to H related defects. Furthermore, OVs with $-/0$ CTLs near the CBM of the substrate tend to have comparably low concentrations and can thus be neglected for electron capture processes. We thus conclude that OVs only play a minor role concerning the electron capture in ultra-scaled devices.

HBs have CTLs in the vicinity of the respective band edges of Si for both electron and hole trapping. Nevertheless, they are only likely to form at preexisting OVs as shown by our formation energy analysis (distributed around 2 eV at preexisting OV compared to 7 eV in SiO_2 bulk) which heavily limits their concentration. According to our calculations, H-E' is the most relevant defect candidate for trapping charges, as its formation energy in the bulk system is in a reasonable energy range ($E_{\mathrm{Form}} = 2.4 \pm 0.5$ eV) with CTLs near the band edges of the Si substrate, effective for both electron and hole capture. Our analysis of the negative charge state shows that by considering only the stable H-E'^{-}_{min} configurations, the H-E' defects have CTLs for trapping electrons distributed around 1.5 ± 0.4 eV below the CBM of the Si substrate. Thus, for this defect type, the interaction with electrons from the conduction band edge of Si is suppressed compared to holes from the valence band edge, with both of the $+/0$ CTLs distributed only around 0.5 ± 0.5 eV above the VBM of the substrate. We therefore claim that the H-E' is a valid defect candidate for causing NBTI, as, furthermore, H-E' defects with CTLs below the VBM of Si also have the lowest formation energies and therefore exist in higher concentrations as well. The comparison between hole and electron capture CTLs gives a good explanation for the suppressed PBTI effect when compared to NBTI observed in MOS devices. By correlating different CTLs of single defects in our multi-state model, we see that two trap levels of the same defect can differ by more than 2 eV, which can directly be linked to different charge capture time constants of single defects observed for example in anomalous random telegraph noise.

The charged energy levels of a defect can be shifted by an applied bias in a MOS structure, altering the Fermi level dependent formation energy and the transition barriers between differently charged configurations. To investigate all occurring charge transitions, relaxation energies were calculated and used as fitting points for potential energy curves (PEC) in the harmonic approximation. By extracting the energy barriers from the crossing points of two differently charged PECs, we show that energy barriers for single charge transfers vary between 0.1 and 2.5 eV depending on the Fermi level. Furthermore, we demonstrate that a transition from charge state $-(+)$ to 0 compared to the direct transition $-(+)$ to $+(-)$ is not only much more likely in terms of the vanishing cross section of 3-particle processes but is also always energetically favored. We thus conclude that a stable positively charged defect (state 2) is highly unlikely to directly transform into the negative charge state ($2 \rightarrow 3'$). Instead, the defect preferably either transitions to a meta-stable puckered configuration without charge transfer ($2 \rightarrow 2'$) or emits a hole to become neutral ($2 \rightarrow 1'$) again. Subsequently, the defect can either once more capture a hole ($1' \rightarrow 2$), undergo a charge conserving transition between puckered and unpuckered ($1' \rightarrow 1$) or, for the relevant H-E', finally trap an electron to transform into one of the negatively charged highly unstable configurations ($1 \rightarrow 3'$), which quickly relax into H-E'^{-}_{min} ($3' \rightarrow 3$). By emitting the extra electron, the H either diffuses away from the defect site ($3 \rightarrow 0$), potentially creating a new defect at a different position in the oxide, or the defect either becomes neutral again ($3 \rightarrow 1$), able to capture either an electron or a hole from the substrate again.

5. Conclusions

This work offers a generalized nonradiative multi-phonon defect model for the defect types oxygen vacancy, hydrogen bridge and hydroxyl-E' center based on large scale and consistent DFT calculations of atomic defects in amorphous SiO_2. Our final model combines both electron and hole capture processes in a unified manner by containing six different defect states, a stable and a metastable configuration in each charge state 0, + and −. The energy barriers for all occurring transitions in this model are analyzed by respectively employing a nudged elastic band method and by calculating relaxation energies of all defects and subsequently employing the harmonic approximation to the potential energy surfaces, revealing that a transition from charge state $-(+)$ to 0 is energetically always favored compared to the direct transition $-(+)$ to $+(-)$. Based on our formation energy analysis, the calculated charge transition levels and experimentally determined oxygen vacancy concentrations, we show that the hydroxyl-E' center (H-E') is the most relevant defect type in a-SiO_2 for causing device degrading phenomena in Si/SiO_2 MOSFETs. We furthermore show that OVs have $+/0$ CTLs near the valence band maximum of SiC, suitable for hole trapping. The varying CTLs of single defects give an explanation for vanishing defects and differing time constants of anomalous random telegraph noise observed in time dependent defect spectroscopy. In the negative charge state, the H-E' center was linked via transition barrier calculations to a stable configuration, were a Si gets fivefold coordinated with four O and one H. This defect state called H-E'^{-}_{min} is on average 1.5 eV lower in energy compared to all other negatively charged H-E' configurations with charge transition levels distributed >1.6 eV below the conduction band edge of Si and SiC substrates of MOS devices. As the $+/0$ charge transition levels are distributed around the valence band maximum of Si, we conclude that capturing holes from the substrate during operation is more pronounced in Si/SiO_2 MOSFETs than capturing electrons. This observation is in good agreement with the reduced positive bias temperature instability (PBTI) effect compared to its negative counterpart (NBTI) observed in Si/SiO_2 MOS devices, as positive gate voltages shift the $-/0$ trapping level even deeper below the band gap of the substrate.

CRediT authorship contribution statement

Christoph Wilhelmer: Conceptualization, Methodology, Data curation, Formal analysis, Software, Visualization, Writing – original draft. **Dominic Waldhoer:** Conceptualization, Methodology, Validation, Software, Writing – review & editing. **Markus Jech:** Conceptualization, Methodology, Validation, Writing – review & editing. **Al-Moatasem Bellah El-Sayed:** Validation, Writing – review & editing. **Lukas Cvitkovich:** Software, Validation. **Michael Waltl:** Funding acquisition, Writing – review & editing. **Tibor Grasser:** Conceptualization, Validation, Funding acquisition, Supervision, Writing – review & editing.

Declaration of competing interest

The authors declare the following financial interests/personal relationships which may be considered as potential competing interests: Christoph Wilhelmer and Michael Waltl report financial support provided by Christian Doppler Laboratories for Single-Defect Spectroscopy in Semiconductor Devices at the Institute for Microelectronics, TU Wien.

Dominic Waldhoer, Markus Jech, Al-Moatasem Bellah El-Sayed, Lukas Cvitkovich and Tibor Grasser report financial support provided by Institute for Microelectronics, TU Wien.

Al-Moatasem Bellah El-Sayed reports financial support provided by Nanolayers Research Computing.

Data availability

Data will be made available on request.

Acknowledgments

The financial support by the Austrian Federal Ministry for Digital and Economic Affairs, the National Foundation for Research, Technology and Development and the Christian Doppler Research Association are gratefully acknowledged. Furthermore, this project was funded by the European Union's Horizon 2020 research and innovation program under grant agreement No. 871813, within the framework of the project Modeling Unconventional Nanoscaled DeviceFABrication (MUNDFAB). The authors acknowledge TU Wien Bibliothek for financial support through its Open Access Funding Programme. We also wish to acknowledge the support from the Vienna Scientific Cluster for providing resources on the Austrian high-performance clusters VSC3 and VSC4.

Appendix. Weibull distribution

The Weibull distribution parametrization used for this work is given by

$$f(E) = \frac{b}{a}\left(\pm\frac{E-c}{a}\right)^{b-1} \mathrm{e}^{-\left(\pm\frac{E-c}{a}\right)^{b}} \tag{A.1}$$

with the scale parameter a, the shape parameter b and the location parameter c. The plus sign before the $(E-c)$ term corresponds to the Weibull minimum distribution employed for the CTLs of OVs while the minus sign corresponds to the Weibull maximum distribution used for the E_{Form} of HBs.

References

[1] M. Jech, A.-M. El-Sayed, S. Tyaginov, A.L. Shluger, T. Grasser, *Ab initio* treatment of silicon-hydrogen bond rupture at Si/SiO_2 interfaces, Phys. Rev. B 100 (2019) 195302, http://dx.doi.org/10.1103/PhysRevB.100.195302.

[2] R.A.B. Devine, J. Arndt, Si—O bond-length modification in pressure-densified amorphous SiO_2, Phys. Rev. B 35 (1987) 9376–9379, http://dx.doi.org/10.1103/PhysRevB.35.9376.

[3] S. Mukhopadhyay, P.V. Sushko, A.M. Stoneham, A.L. Shluger, Modeling of the structure and properties of oxygen vacancies in amorphous silica, Phys. Rev. B 70 (2004) 195203, http://dx.doi.org/10.1103/PhysRevB.70.195203.

[4] F. Schanovsky, O. Baumgartner, V. Sverdlov, T. Grasser, A multi scale modeling approach to non-radiative multi phonon transitions at oxide defects in MOS structures, J. Comput. Electron. 11 (2012) http://dx.doi.org/10.1007/s10825-012-0403-1.

[5] A.-M. El-Sayed, M.B. Watkins, V.V. Afanas'ev, A.L. Shluger, Nature of intrinsic and extrinsic electron trapping in SiO_2, Phys. Rev. B 89 (2014) 125201, http://dx.doi.org/10.1103/PhysRevB.89.125201.

[6] S. Dannefaer, T. Bretagnon, D. Kerr, Vacancy-type defects in crystalline and amorphous SiO_2, J. Appl. Phys. 74 (2) (1993) 884–890, http://dx.doi.org/10.1063/1.354882.

[7] G. Pacchioni, L. Skuja, D. Griscom, Defects in SiO_2 and Related Dielectrics: Science and Technology, 2000, http://dx.doi.org/10.1007/978-94-010-0944-7.

[8] T. Grasser, H. Reisinger, P.-J. Wagner, B. Kaczer, Time-dependent defect spectroscopy for characterization of border traps in metal-oxide-semiconductor transistors, Phys. Rev. B 82 (2010) 245318, http://dx.doi.org/10.1103/PhysRevB.82.245318.

[9] B.K. Park, J. Park, M. Cho, C.S. Hwang, K. Oh, Y. Han, D.Y. Yang, Interfacial reaction between chemically vapor-deposited HfO_2 thin films and a HF-cleaned Si substrate during film growth and postannealing, Appl. Phys. Lett. 80 (13) (2002) 2368–2370, http://dx.doi.org/10.1063/1.1466534.

[10] T.L. Duan, L. Pan, Z. Zhang, E.S. Tok, J.S. Pan, Characterization of the electronic structure and thermal stability of HfO_2/SiO_2/Si gate dielectric stack, Surf. Interface Anal. 49 (8) (2017) 776–780, http://dx.doi.org/10.1002/sia.6222.

[11] G. Rzepa, J. Franco, B. O'Sullivan, A. Subirats, M. Simicic, G. Hellings, P. Weckx, M. Jech, T. Knobloch, M. Waltl, P. Roussel, D. Linten, B. Kaczer, T. Grasser, Comphy — A compact-physics framework for unified modeling of BTI, Microelectron. Reliab. 85 (2018) 49–65, http://dx.doi.org/10.1016/j.microrel.2018.04.002.

[12] Y. Wimmer, A.-M. El-Sayed, W. Goes, T. Grasser, A.L. Shluger, Role of hydrogen in volatile behavior of defects in SiO_2-based electronic devices, Proc. R. Soc. Lond. Ser. A Math. Phys. Eng. Sci. 472 (2190) (2016) 20160009, http://dx.doi.org/10.1098/rspa.2016.0009.

[13] T. Grasser, B. Kaczer, W. Goes, H. Reisinger, T. Aichinger, P. Hehenberger, P. Wagner, F. Schanovsky, J. Franco, M.T. Toledano Luque, M. Nelhiebel, The paradigm shift in understanding the bias temperature instability: From reaction–diffusion to switching oxide traps, IEEE Trans. Electron. Devices 58 (11) (2011) 3652–3666, http://dx.doi.org/10.1109/TED.2011.2164543.

[14] T. Grasser, Stochastic charge trapping in oxides: From random telegraph noise to bias temperature instabilities, Microelectron. Reliab. 52 (1) (2012) 39–70, http://dx.doi.org/10.1016/j.microrel.2011.09.002.

[15] Z.-Y. Lu, C.J. Nicklaw, D.M. Fleetwood, R.D. Schrimpf, S.T. Pantelides, Structure, properties, and dynamics of oxygen vacancies in amorphous SiO_2, Phys. Rev. Lett. 89 (2002) 285505, http://dx.doi.org/10.1103/PhysRevLett.89.285505.

[16] P. Sushko, S. Mukhopadhyay, A. Stoneham, A. Shluger, Oxygen vacancies in amorphous silica: Structure and distribution of properties, Microelectron. Eng. 80 (2005) 292–295, http://dx.doi.org/10.1016/j.mee.2005.04.083.

[17] F. Schanovsky, O. Baumgartner, W. Goes, T. Grasser, A detailed evaluation of model defects as candidates for the bias temperature instability, in: 2013 International Conference on Simulation of Semiconductor Processes and Devices (SISPAD), 2013, pp. 1–4, http://dx.doi.org/10.1109/SISPAD.2013.6650559.

[18] D. Waldhoer, C. Schleich, J. Michl, B. Stampfer, K. Tselios, E.G. Ioannidis, H. Enichlmair, M. Waltl, T. Grasser, Toward automated defect extraction from bias temperature instability measurements, IEEE Trans. ELectron Devices 68 (8) (2021) 4057–4063, http://dx.doi.org/10.1109/TED.2021.3091966.

[19] W. Goes, Y. Wimmer, A.-M. El-Sayed, G. Rzepa, M. Jech, A. Shluger, T. Grasser, Identification of oxide defects in semiconductor devices: A systematic approach linking DFT to rate equations and experimental evidence, Microelectron. Reliab. 87 (2018) 286–320, http://dx.doi.org/10.1016/j.microrel.2017.12.021.

[20] C. Schleich, D. Waldhoer, K. Waschneck, M.W. Feil, H. Reisinger, T. Grasser, M. Waltl, Physical modeling of charge trapping in 4H-SiC DMOSFET technologies, IEEE Trans. Electron Devices 68 (8) (2021) 4016–4021, http://dx.doi.org/10.1109/TED.2021.3092295.

[21] A.-M. El-Sayed, M.B. Watkins, T. Grasser, V.V. Afanas'ev, A.L. Shluger, Hydrogen-induced rupture of strained Si—O bonds in amorphous silicon dioxide, Phys. Rev. Lett. 114 (2015) 115503, http://dx.doi.org/10.1103/PhysRevLett.114.115503.

[22] A.-M. El-Sayed, Y. Wimmer, W. Goes, T. Grasser, V.V. Afanas'ev, A.L. Shluger, Theoretical models of hydrogen-induced defects in amorphous silicon dioxide, Phys. Rev. B 92 (2015) 014107, http://dx.doi.org/10.1103/PhysRevB.92.014107.

[23] M. Kaviani, V.V. Afanas'ev, A.L. Shluger, Interactions of hydrogen with amorphous hafnium oxide, Phys. Rev. B 95 (2017) 075117, http://dx.doi.org/10.1103/PhysRevB.95.075117.

[24] A. Iino, M. Kuwabara, K. Kokura, Mechanisms of hydrogen-induced losses in silica-based optical fibers, J. Lightwave Technol. 8 (11) (1990) 1675–1679, http://dx.doi.org/10.1109/50.60564.

[25] J. Stone, J.M. Wiesenfeld, D. Marcuse, C.A. Burrus, S. Yang, Formation of hydroxyl due to reaction of hydrogen with silica optical fiber preforms, Appl. Phys. Lett. 47 (3) (1985) 328–330, http://dx.doi.org/10.1063/1.96152.

[26] M. Stuckelberger, R. Biron, N. Wyrsch, F.-J. Haug, C. Ballif, Review: Progress in solar cells from hydrogenated amorphous silicon, Renew. Sustain. Energy Rev. 76 (2017) 1497–1523, http://dx.doi.org/10.1016/j.rser.2016.11.190.

[27] H. Nagayoshi, Y. Onozawa, M. Ikeda, M. Yamaguchi, Y. Yamamoto, T. Uematsu, T. Saitoh, K. Kamisako, Effect of hydrogen-radical annealing for SiO_2 passivation, Jpn. J. Appl. Phys. 35 (Part 2, No. 8B) (1996) L1047–L1049, http://dx.doi.org/10.1143/jjap.35.l1047.

[28] C. Kaneta, T. Yamasaki, T. Uchiyama, T. Uda, K. Terakura, Defect states due to silicon dangling bonds at the Si(100)/SiO_2 interface and the passivation by hydrogen atoms, MRS Proc. 592 (1999) 39, http://dx.doi.org/10.1557/PROC-592-39.

[29] F. Messina, M. Cannas, Character of the reaction between molecular hydrogen and a silicon dangling bond in amorphous SiO_2, J. Phys. Chem. C 111 (18) (2007) 6663–6667, http://dx.doi.org/10.1021/jp0705727.

[30] A. Stesmans, Interaction of P_b defects at the (111)Si/SiO_2 interface with molecular hydrogen: Simultaneous action of passivation and dissociation, J. Appl. Phys. 88 (1) (2000) 489–497, http://dx.doi.org/10.1063/1.373684.

[31] P. Avouris, R. Walkup, A. Rossi, T.-C. Shen, G. Abeln, J. Tucker, J. Lyding, STM-induced H atom desorption from Si(100): Isotope effects and site selectivity, Chem. Phys. Lett. 257 (1) (1996) 148–154, http://dx.doi.org/10.1016/0009-2614(96)00518-0.

[32] A.T. Krishnan, S. Chakravarthi, P. Nicollian, V. Reddy, S. Krishnan, Negative bias temperature instability mechanism: The role of molecular hydrogen, Appl. Phys. Lett. 88 (15) (2006) 153518, http://dx.doi.org/10.1063/1.2191828.

[33] C. Wilhelmer, M. Jech, D. Waldhör, A.-M. El-Sayed, L. Cvitkovich, T. Grasser, Statistical ab initio analysis of electron trapping oxide defects in the Si/SiO_2 network, in: Proceedings of the European Solid-STate Device Research Conference (ESSDERC), 2021, pp. 243–246, http://dx.doi.org/10.1109/ESSDERC53440.2021.9631833.

[34] L. Skuja, K. Kajihara, M. Hirano, A. Saitoh, H. Hosono, An increased F_2-laser damage in 'wet' silica glass due to atomic hydrogen: A new hydrogen-related E'-center, J. Non-Cryst. Solids 352 (23) (2006) 2297–2302, http://dx.doi.org/10.1016/j.jnoncrysol.2006.01.101.

[35] A.-M. El-Sayed, M.B. Watkins, T. Grasser, V.V. Afanas'ev, A.L. Shluger, Hole trapping at hydrogenic defects in amorphous silicon dioxide, Microelectron. Eng. 147 (2015) 141–144, http://dx.doi.org/10.1016/j.mee.2015.04.073.

[36] J. Isoya, J.A. Weil, L.E. Halliburton, EPR and *ab initio* SCF-MO studies of the Si·H-Si system in the E_4' center of α-quartz, J. Chem. Phys. 74 (1981) 5436–5448, http://dx.doi.org/10.1063/1.440948.

[37] R.A. Weeks, C.M. Nelson, Trapped electrons in irradiated quartz and silica: II, electron spin resonance, J. Am. Ceram. Soc. 43 (8) (2006) 399–404, http://dx.doi.org/10.1111/j.1151-2916.1960.tb13682.x.

[38] J.F. Conley, P.M. Lenahan, A.J. Lelis, T.R. Oldham, Electron spin resonance evidence for the structure of a switching oxide trap: Long term structural change at silicon dangling bond sites in SiO_2, Appl. Phys. Lett. 67 (15) (1995) 2179–2181, http://dx.doi.org/10.1063/1.115095.

[39] Y. Yue, Y. Song, X. Zuo, First principles study of oxygen vacancy defects in amorphous SiO_2, AIP Adv. 7 (1) (2017) 015309, http://dx.doi.org/10.1063/1.4975147.

[40] T.D. Kühne et al., CP2K: An electronic structure and molecular dynamics software package - Quickstep: Efficient and accurate electronic structure calculations, J. Chem. Phys. 152 (19) (2020) 194103, http://dx.doi.org/10.1063/5.0007045.

[41] S. Goedecker, M. Teter, J. Hutter, Separable dual-space Gaussian pseudopotentials, Phys. Rev. B 54 (1996) 1703–1710, http://dx.doi.org/10.1103/PhysRevB.54.1703.

[42] J. Van de Vondele, J. Hutter, Gaussian basis sets for accurate calculations on molecular systems in gas and condensed phases, J. Chem. Phys. 127 (11) (2007) 114105, http://dx.doi.org/10.1063/1.2770708.

[43] M. Guidon, J. Hutter, J. Van de Vondele, Robust periodic hartree-fock exchange for large-scale simulations using Gaussian basis sets, J. Chem. Theory Comput. 5 (11) (2009) 3010–3021, http://dx.doi.org/10.1021/ct900494g.

[44] M. Guidon, J. Hutter, J. Van de Vondele, Auxiliary density matrix methods for hartree-fock exchange calculations, J. Chem. Theory Comput. 6 (2010) 2348–2364, http://dx.doi.org/10.1021/ct1002225.

[45] G. Henkelman, B.P. Uberuaga, H. Jónsson, A climbing image nudged elastic band method for finding saddle points and minimum energy paths, J. Chem. Phys. 113 (22) (2000) 9901–9904, http://dx.doi.org/10.1063/1.1329672.

[46] S. Plimpton, Fast parallel algorithms for short-range molecular dynamics, J. Comput. Phys. 117 (1) (1995) 1–19, http://dx.doi.org/10.1006/jcph.1995.1039.

[47] A. Van Duin, A. Strachan, S. Stewman, Q. Zhang, X. Xu, W. Goddard, $ReaxFF_{SiO}$ reactive force field for silicon and silicon oxide systems, J. Phys. Chem. A 107 (19) (2003) 3803–3811, http://dx.doi.org/10.1021/jp0276303.

[48] C.G. Broyden, The convergence of a class of double-rank minimization algorithms 1. general considerations, IMA J. Appl. Math. 6 (1) (1970) 76–90, http://dx.doi.org/10.1093/imamat/6.1.76.

[49] R. Fletcher, A new approach to variable metric algorithms, Comput. J. 13 (3) (1970) 317–322, http://dx.doi.org/10.1093/comjnl/13.3.317.

[50] D. Goldfarb, A family of variable-metric methods derived by variational means, Math. Comp. 24 (109) (1970) 23–26, http://dx.doi.org/10.1090/S0025-5718-1970-0258249-6.

[51] D.F. Shanno, Conditioning of quasi-Newton methods for function minimization, Math. Comp. 24 (111) (1970) 647–656, http://dx.doi.org/10.1090/S0025-5718-1970-0274029-X.

[52] S. Kohara, K. Suzuya, Intermediate-range order in vitreous SiO_2 and GeO_2, J. Condens. Matter Phys. 17 (5) (2005) S77–S86, http://dx.doi.org/10.1088/0953-8984/17/5/009.

[53] B. El-Kareh, Fundamentals of Semiconductor Processing Technology, Springer US, Boston, 1995, http://dx.doi.org/10.1007/978-1-4615-2209-6.

[54] S.R. Elliott, Physics of Amorphous Materials/ S.R. Elliott, Longman Scientific & Technical, New York, 1984, http://dx.doi.org/10.1002/crat.2170200922.

[55] D. Price, J. Carpenter, Scattering function of vitreous silica, J. Non-Cryst. Solids 92 (1) (1987) 153–174, http://dx.doi.org/10.1016/S0022-3093(87)80366-6.

[56] E. Bersch, M. Di, S. Consiglio, R.D. Clark, G.J. Leusink, A.C. Diebold, Complete band offset characterization of the HfO_2/SiO_2/Si stack using charge corrected X-ray photoelectron spectroscopy, J. Appl. Phys. 107 (4) (2010) 043702, http://dx.doi.org/10.1063/1.3284961.

[57] T.E. Cook, C.C. Fulton, W.J. Mecouch, K.M. Tracy, R.F. Davis, E.H. Hurt, G. Lucovsky, R.J. Nemanich, Measurement of the band offsets of SiO_2 on clean *n*- and *p*-type GaN(0001), J. Appl. Phys. 93 (7) (2003) 3995–4004, http://dx.doi.org/10.1063/1.1559424.

[58] E. Bersch, S. Rangan, R.A. Bartynski, E. Garfunkel, E. Vescovo, Band offsets of ultrathin high-κ oxide films with Si, Phys. Rev. B 78 (2008) 085114, http://dx.doi.org/10.1103/PhysRevB.78.085114.

[59] A.J. Garza, G.E. Scuseria, Predicting band gaps with hybrid density functionals, J. Phys. Chem. Lett. 7 (20) (2016) 4165–4170, http://dx.doi.org/10.1021/acs.jpclett.6b01807.

[60] T.-H. Kil, K. Kita, Anomalous band alignment change of SiO_2/4H–SiC (0001) and (000–1) MOS capacitors induced by NO-POA and its possible origin, Appl. Phys. Lett. 116 (12) (2020) 122103, http://dx.doi.org/10.1063/1.5135606.

[61] R. Mahapatra, A.K. Chakraborty, A.B. Horsfall, N.G. Wright, G. Beamson, K.S. Coleman, Energy-band alignment of HfO_2/SiO_2/SiC gate dielectric stack, Appl. Phys. Lett. 92 (4) (2008) 042904, http://dx.doi.org/10.1063/1.2839314.

[62] V.V. Afanas'ev, M. Bassler, G. Pensl, M.J. Schulz, E. Stein von Kamienski, Band offsets and electronic structure of SiC/SiO_2 interfaces, J. Appl. Phys. 79 (6) (1996) 3108–3114, http://dx.doi.org/10.1063/1.361254.

[63] T. Grasser, W. Goes, Y. Wimmer, F. Schanovsky, G. Rzepa, M. Waltl, K. Rott, H. Reisinger, V. Afanas'ev, A. Stesmans, A.-M. El-Sayed, A. Shluger, On the microscopic structure of hole traps in pMOSFETs, in: 2014 IEEE International Electron Devices Meeting, 2014, pp. 21.1.1–21.1.4, http://dx.doi.org/10.1109/IEDM.2014.7047093.

[64] A. Kimmel, P. Sushko, A. Shluger, G. Bersuker, Positive and negative oxygen vacancies in amorphous silica, ECS Trans. 19 (2) (2009) 3–17, http://dx.doi.org/10.1149/1.3122083.

[65] Y.-Y. Liu, F. Liu, R. Wang, J.-W. Luo, X. Jiang, R. Huang, S.-S. Li, L.-W. Wang, Characterizing the charge trapping across crystalline and amorphous Si/SiO_2/HfO_2 stacks from first-principle calculations, Phys. Rev. Appl. 12 (2019) 064012, http://dx.doi.org/10.1103/PhysRevApplied.12.064012.

[66] Y.-Y. Liu, F. Zheng, X. Jiang, J.-W. Luo, S.-S. Li, L.-W. Wang, Ab initio investigation of charge trapping across the crystalline-Si–amorphous-SiO_2 interface, Phys. Rev. Appl. 11 (2019) 044058, http://dx.doi.org/10.1103/PhysRevApplied.11.044058.

[67] P.E. Blöchl, First-principles calculations of defects in oxygen-deficient silica exposed to hydrogen, Phys. Rev. B 62 (2000) 6158–6179, http://dx.doi.org/10.1103/PhysRevB.62.6158.

[68] J. Godet, A. Pasquarello, *Ab initio* study of charged states of H in amorphous SiO_2, Microelectron. Eng. 80 (2005) 288–291, http://dx.doi.org/10.1016/j.mee.2005.04.082, 14th biennial Conference on Insulating Films on Semiconductors.

[69] C.G. Van de Walle, J. Neugebauer, First-principles calculations for defects and impurities: Applications to III-nitrides, J. Appl. Phys. 95 (8) (2004) 3851–3879, http://dx.doi.org/10.1063/1.1682673.

[70] G. Makov, M.C. Payne, Periodic boundary conditions in *ab initio* calculations, Phys. Rev. B 51 (1995) 4014–4022, http://dx.doi.org/10.1103/PhysRevB.51.4014.

[71] C. Freysoldt, J. Neugebauer, C.G. Van de Walle, Fully *ab initio* finite-size corrections for charged-defect supercell calculations, Phys. Rev. Lett. 102 (2009) 016402, http://dx.doi.org/10.1103/PhysRevLett.102.016402.

[72] D.Z. Gao, J. Strand, M.S. Munde, A.L. Shluger, Mechanisms of oxygen vacancy aggregation in SiO_2 and HfO_2, Front. Phys. 7 (43) (2019) http://dx.doi.org/10.3389/fphy.2019.00043.

[73] R.A.B. Devine, J. Arndt, Defect pair creation through ultraviolet radiation in dense, amorphous SiO_2, Phys. Rev. B 42 (1990) 2617–2620, http://dx.doi.org/10.1103/PhysRevB.42.2617.

[74] G. Buscarino, S. Agnello, Experimental evidence of E'_γ centers generation from oxygen vacancies in a-SiO_2, J. Non-Cryst. Solids 353 (5) (2007) 577–580, http://dx.doi.org/10.1016/j.jnoncrysol.2006.12.031.

[75] C. Parks, B. Robinson, H. Leary, K. Childs, G. Coyle, The chemical interface of microwave plasma deposited SiO_2 films, MRS Proc. 105 (1987) http://dx.doi.org/10.1557/PROC-105-133.

[76] N.H. Nickel, Hydrogen diffusion through silicon/silicon dioxide interfaces, J. Vac. Sci. Technol. B 18 (3) (2000) 1770–1772, http://dx.doi.org/10.1116/1.591469.

[77] D. Waldhör, A.-M. El-Sayed, Y. Wimmer, M. Waltl, T. Grasser, Atomistic modeling of oxide defects, in: T. Grasser (Ed.), Noise in Nanoscale Semiconductor Devices, Springer International Publishing, 2020, pp. 609–648, http://dx.doi.org/10.1007/978-3-030-37500-3{_}18.

[78] M.J. Uren, M.J. Kirton, S. Collins, Anomalous telegraph noise in small-area silicon metal-oxide-semiconductor field-effect transistors, Phys. Rev. B 37 (1988) 8346–8350, http://dx.doi.org/10.1103/PhysRevB.37.8346.

[79] A. Lelis, T. Oldham, Time dependence of switching oxide traps, IEEE Trans. Nucl. Sci. 41 (6) (1994) 1835–1843, http://dx.doi.org/10.1109/23.340515.

[80] B.E. Deal, A.S. Grove, General relationship for the thermal oxidation of silicon, J. Appl. Phys. 36 (12) (1965) 3770–3778, http://dx.doi.org/10.1063/1.1713945.

[81] J. Franco, H. Arimura, J. Marneffe, Z. Wu, A. Vandooren, L. Ragnarsson, E.D. Litta, N. Horiguchi, K. Croes, D. Linten, V. Afanas'ev, T. Grasser, B. Kaczer, Low-temperature atomic and molecular hydrogen anneals for enhanced chemical SiO_2 IL quality in low thermal budget RMG stacks, in: 2021 IEEE International Electron Devices Meeting (IEDM), 2021, pp. 31.4.1–31.4.4, http://dx.doi.org/10.1109/IEDM19574.2021.9720657.